Ash Density and Trabecular Bone Structure in Proximal Femur Fracture

Ash Density and Trabecular Bone Structure in Proximal Femur Fracture

by

Chris Milburn

A Thesis
Submitted to the School of Graduate Studies
in Partial Fulfillment of the Requirements
for the degree
Master of Science
in Physics

McMaster University
August 1993

Master of Science (1993) McMaster University
(Medical Physics) Hamilton, Ont.

Title: Trabecular Bone Structure and Density
in Proximal Femur Fracture

Author: Chris Milburn

Supervisor: Dr. C.E. Webber

Number of Pages: x, 90

Abstract

The likelihood of a given bone fracturing atraumatically is difficult to assess.. A number of factors - age, frequency of falling, cushioning by overlying tissues, protective reactions - as well as bone strength determine fracture risk. The interrelationships between these factors make it hard to evaluate the effect of any one variable in a study.

The most common method of assessing bone strength is to use the surrogate method of bone mineral content (BMC) or bone mineral density (BMD). The architectural breakdown of the trabeculae, the mineral "mesh" which makes up bone, is a little-studied factor which may help to better predict fracture. In this thesis, the results of quantitative measurements of trabecular architecture, BMD, and strength of femoral heads scavenged from hip replacement surgery will be presented. This is intended to illuminate the relationships between bone strength, bone density, and trabecular architecture.

Acknowledgements

I have a huge number of people to thank for helping me through this work, but firstly I must anti-acknowledge the beaurocratic system at MUMC which made it possible for me to wait so long without getting any samples to work with. I am quite sure the system is under the control of hostile aliens. Why else would they give me my first sample 2 weeks after I had finished experiments?

Firstly, thanks to Dave Libby who helped me with computer things and provided me with much-needed abuse.

Having successfully worked in Pathology, Electron Microscopy, and materials testing, all of which I was (am) totally ignorant of, I obviously got a lot of help in these areas. A thousand thank-you's to John Hamilton in pathology for the use of the equipment and all his help. Muchos gracias to Ed McCaffery in materials testing for showing me how to set up and use the equipment about 6 times.

The biggest thank-you goes to Dr. Larry Arsenault in Electron Microscopy, who not only allowed me to use his image analysis system but also helped me analyze my samples, which God knows I couldn't have done by myself. Without him this thesis would have taken a completely different path.

Thanks very much to Drs. Riddell and Smith for their help in procuring bone samples from MUMC. Thanks very much to Nancy and the rest of the pathology department at Hotel Dieu in St. Catherine's for getting me the bulk of my samples.

Thanks to my good friend Ricky whose help and practical philosophical advice made my time here at Mac so enjoyable.

To my roommates Pat, Gord, Mark, Marlene, Heather, and Andrew, thanks for being part of what was always a wonderful environment to come home to. Special thanks to Pete for showing me that it is possible, if necessary, to do a complete Master's thesis, albeit a hurtin' one, in less than two weeks. Thanks, too, for being a great friend. Peace and No Meat!

To my brother Doug and his fiancee Michelle, thank you so much for scheduling your wedding right at the time when I hoped to wrap up, thereby spurring me on to finish.

Thank you Mom and Dad for your encouragement, love and understanding. It's nice to know there's someone who will always be there for you.

Thank you to my wonderful girlfriend Stephanie for helping me

through the bad times and being here to help me enjoy the good times more. I never would have made it without you.

Thanks very much to the members of my committee, Dr. Chettle and Dr. Adachi, for their guidance. Particular thanks to Dr. Adachi for his help in getting bone samples and with the pQCT section of this work.

Finally, I have to thank the best supervisor in the world, Dr. Webber. I don't imagine I'll ever again have the opportunity to work with and know a better person.

Table of Contents

List of Illustrations

List of Tables

Chapter 1
An Introduction to Osteoporosis

1.1 Overview

Osteoporosis is a serious problem, the costs of which have been estimated at more than 7 billion dollars per year in the USA [1]. The three most common fractures associated with osteoporosis are Colles fracture (fracture of the wrist), vertebral crush fracture, and hip (proximal femur) fracture. Other fracture sites are the humerus or pelvis, or other less common locations. With sufficient force, these fractures can occur in anyone, but are considered osteoporotic when they occur in the elderly or as a result of minimal trauma. The skeletal locations of the three most common fracture sites are shown in figure 1.1.

Hip fracture is by far the most costly and debilitating of osteoporotic fractures. Approximately 210,000 hip fractures occur yearly in the U.S.A. Average time of hospitalization is 3 weeks. Mortality rate in the first year is elevated 12-20% (above normal, nonfractured persons). Many victims suffer permanent physical

Figure 1.1

Taken From "The Anatomy Coloring Book"

Skeletal Locations of the Three Common Osteoporotic Fractures

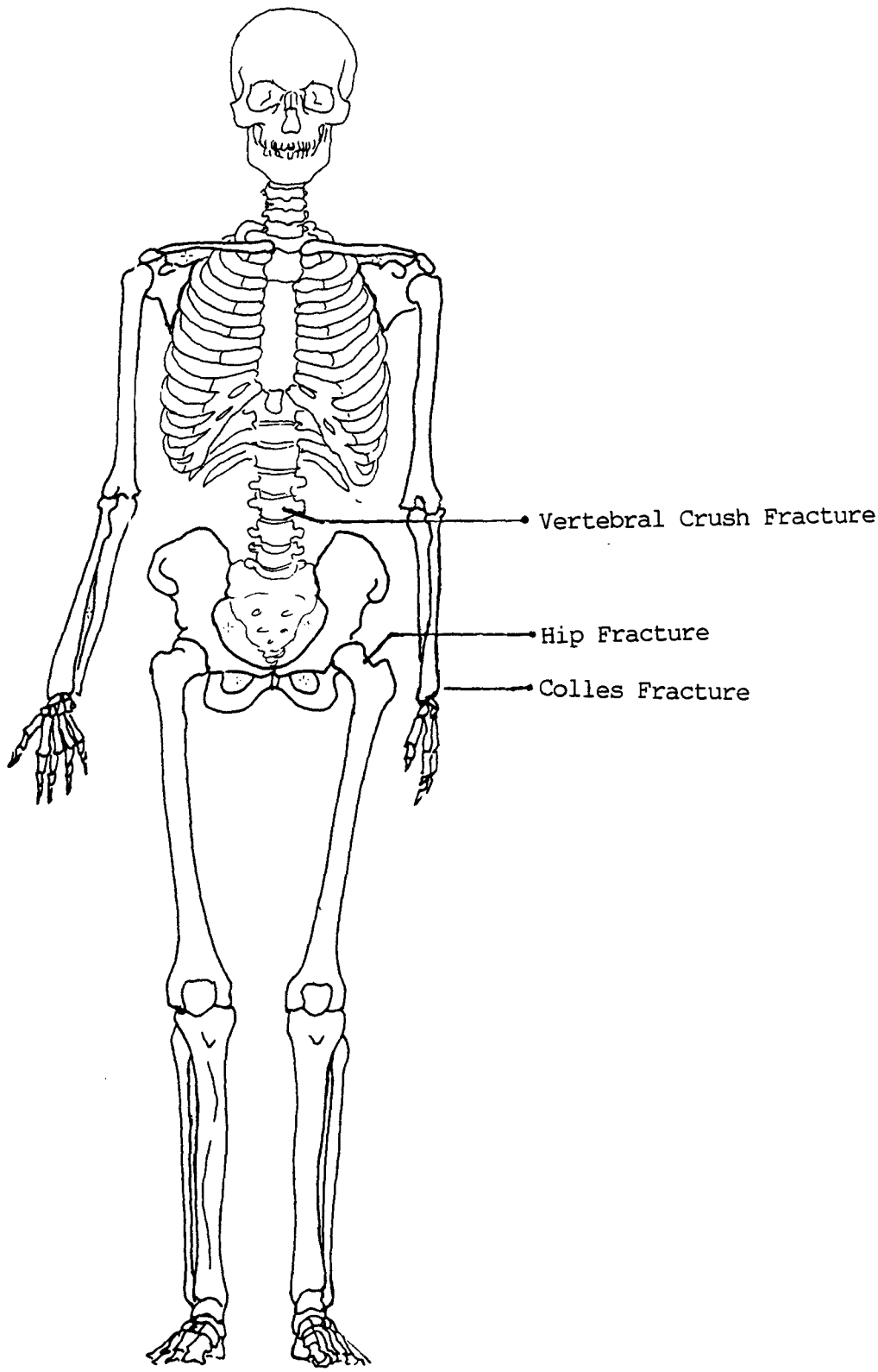

impairment and can never resume their previous lifestyle [2].

The name "hip" fracture is actually somewhat misleading to the layman since it is not one of the bones of the pelvis (ilium, ischium, or pubis) which fractures, but rather the proximal end of the long bone of the thigh - the femur.

Females are much more at risk than males for this injury (75-80% of hip fractures affect women). Hip fracture incidence equalizes somewhat between the sexes in the very elderly (80 years of age and over) [2, 3].

A common misconception is that hip fractures in the elderly can be explained completely by osteoporosis. Osteoporosis is defined as "a porosity and brittleness of the bones due to loss of protein from the bone matrix" (Collins English Dictionary), the accepted consequence of which is increased fracture risk. A loss of protein will inevitably occur with a loss of bone mineral, which can be measured as a decreased bone mass. Although this is undoubtedly an important factor in elevating fracture risk, it is an incomplete explanation of why elderly people fracture.

A more comprehensive list of the variables which might contribute to an individual's hip fracture risk are:

1) Age
2) Falling frequency
3) Bone strength
4) Overlying Tissues
5) Protective reactions

Age is strongly correlated with hip fracture risk. Older people fracture more often, the relationship between incidence and age

being approximately exponential for hip fracture [2] as shown in figure 1.2. Is the increasing fracture risk due to loss of bone mass, decrease in bone strength, increase in falling, decrease in overlying tissues, or deteriorating protective reactions? It is most likely a combination of all. But simply basing a risk on age would be an incomplete analysis, not differentiating between subgroups in the same age group (athletic vs. non-athletic, fat vs. thin).

There is some epidemiological data on falling frequency. It suggests that the percentage of individuals who fall increases with age after age 60. The risk is considerably higher for females, equalizing somewhat between the sexes around age 75 [4, 5]. Fifty percent of elderly persons who fall do so repeatedly. In the elderly, an estimated 5-10% of falls result in serious injury other than fracture. 5% result in fracture. Approximately one-fifth of these fractures are hip fractures. It is difficult to say whether a given hip fracture results from or causes a fall, but it is estimated that 80-90% of hip fractures result from falls [6]. Thus falling frequency is a variable which influences fracture risk.

It is thought that bone strength is principally determined by bone mass [7], which can be quantified by various methods: QCT (Quantitative Computed Tomography), DPA (Dual Photon Absorptiometry), SPA (Single Photon Absorptiometry), and speed of sound measurements. These techniques and their relative merits have recently been reviewed [8]. There is no doubt that bigger bones are stronger bones and are less prone to fracture.

Overlying tissue is almost totally overlooked in fracture risk studies, despite the fact that it is likely quite an important factor. The presence of fat and (probably more importantly) muscle around a bone will do much to protect the bone in the event of a fall.

Protective reactions refer to an individual's ability, in the event

Figure 1.2

Fracture Incidence vs. Age Showing

Exponential Increase in hip Fractures

From: S.R. Cummings, J.L. Kelsey, M.C. Nevitt, K.J. O'Dowd, "Epidemiology of Osteoporosis and Osteoporotic Fractures", Epidemiologic Reviews, 7, 1985: 178-199.

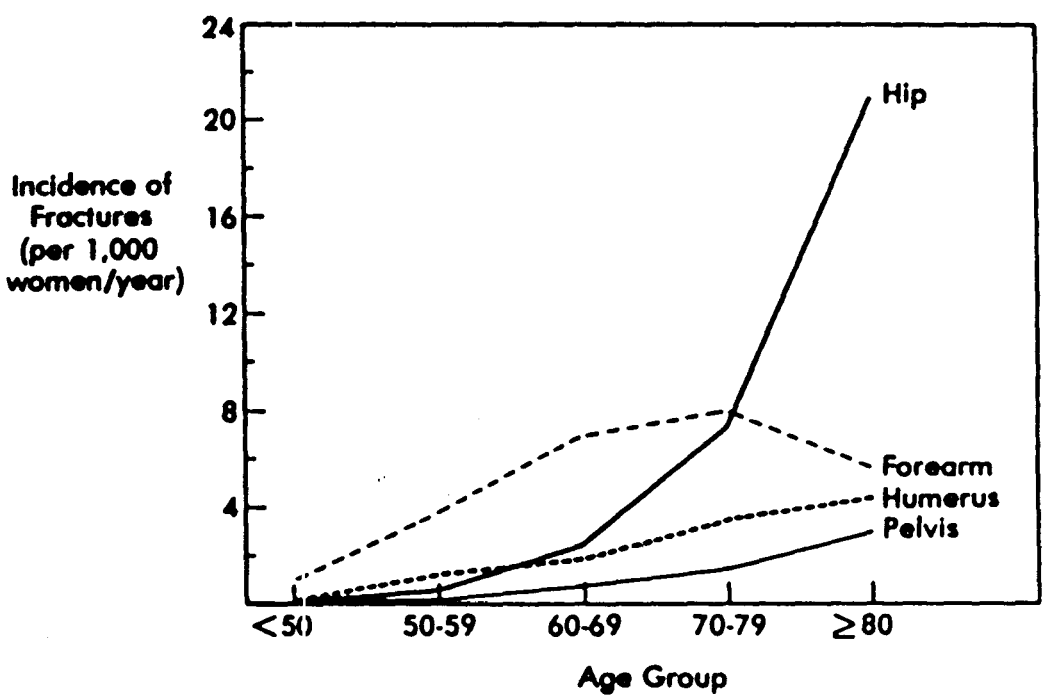

of a fall, to manoeuvre himself while falling to minimize injury. These reactions presumably decrease with age, decreased flexibility or muscle mass, increased drug use, and possibly other factors.

1.2 Interdependency of Variables Influencing Osteoporosis

It is difficult to single out any one factor in a study to measure its effect on fracture risk. In trying to base a risk estimate on bone mass, the picture is always muddied, since people with lower bone mass are usually older or less healthy [9]. This perhaps leads to:
1) an increased number of falls due to lack of reflexes, balance, coordination or muscle strength;
2) loss of protective reactions in the event of a fall (throwing the arms out, rolling over) and
3) less overlying tissue. Younger, healthier individuals would tend to have more tissue, especially muscle, over the hip.

Interestingly, the fact that low bone mass is associated with generally poor health could cause an underestimation of the dependence of fracture risk on bone mass [9]. An individual with decreased bone mass has a higher mortality risk and thus is less likely to suffer a fracture.

A good example of the difficulties intertwined factors present to researchers is the study of the benefits of exercise in combating osteoporosis [10]. The presumed mechanism was that exercise leads to increased bone mass, stronger bones, and a decreased fracture risk. But exercises can potentially affect more than bone mass. Muscles become stronger and larger (overlying tissue factor), balance, coordination and strength increase (frequency of falling/

protective reaction factors). Thus in a group which exercises more frequently and shows lower fracture incidence, we cannot attribute this change solely to bone mass differences that may be present.

Despite the multiplicity of factors described above, bone mass is significantly related to fracture risk [11]. However, there is sufficient uncertainty to warrant further investigation as shown by the scatter in figure 1.3 which compares femoral neck BMD in patients with hip fracture to BMC in non-fracture controls [12]. Trabecular architecture and bone strength may not be simply related to bone mineral density and might be independent estimators of fracture risk, as suggested by several studies [13, 14].

It is possible for example that "nodal density", or the number of trabecular connection points per cm^2 (in a 2-D projected image), is a quantitative factor which can be used to improve fracture risk estimates. A strut structure with a higher nodal density than another will be stronger, even if the two are composed of similar amounts of material.

Support for this work comes from Mielke et. al. [15] who found changes in trabecular bone architecture unrelated to ash density, and Kranendonk [16] who found trabecular pattern uncorrelated with bone mass. This suggests that bone mass cannot be the sole predictor of fracture risk. In a recent paper [17] Jensen et. al. conclude "...measured bone mass should not be the sole indicator of trabecular bone biomechanical competence (stiffness and stress). It is crucial that measurements of bone density are considered in combination with a detailed description of the architecture." They cite their own previous studies in which they found "...decline in bone strength...much exceeded the decline in apparent bone density". Another study [13] states "...age-related structural changes other than bone mass affect the vertebral bone strength strongly." A

Figure 1.3

Hip Fractures

From Riggs et. al [13]

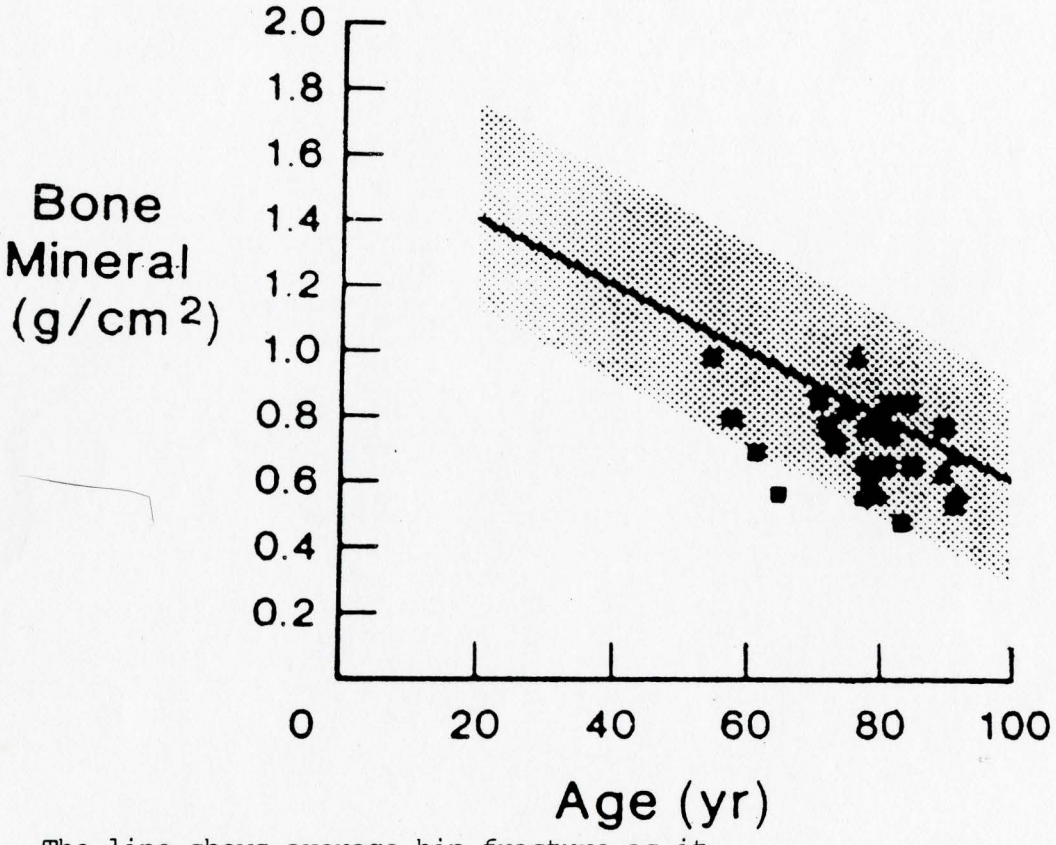

The line shows average hip fracture as it varies with age
The shaded area is one SD on either side of the line
Hip fracture cases are represented by the points
Note that not all hip fracture victims show low bone density.

further study [14] has shown that when compressive strength is plotted against ash density of a bone, there is a considerable spread of values, indicating that other factors determine bone strength besides bone mineral. Many years ago, Singh [18] developed a method of subjectively grading architecture to quantify osteoporotic degradation in the proximal femur. This method proved to be clinically useful in experienced hands.

1.3 Study Purpose and Design

This study is designed to illuminate the relationships between bone mass, bone architecture, and bone strength. Femoral heads will be obtained from hip replacement surgery. Two cores and one thin slice will be taken from the bone sample. One core will be analyzed to determine its mineral density. The other core will be analyzed to determine its mechanical strength. An x-ray of the thin slice will be computer analyzed to determine nodal density. From such measurements in a number of samples, statistical analyses will be used to determine the interrelationships between the three variables. Several possibilities exist:

1) Bone mass correlates strongly with Nodal Density (ND). In this case, no further information could be obtained from measurements of nodal density that is not already provided by measuring bone mass.

2) ND does not correlate well with bone mass or bone strength. In this case, measurements of ND would provide no useful information in assessing fracture risk.

3) ND does not correlate well with bone mass, but does correlate well with bone strength. In this case, measurements of ND could be

used to improve estimates of fracture risk

.

If, as seems likely, our in vitro work supports the concept that an assessment of trabecular architecture would improve our ability to quantitate fracture risk, the question arises as to how architecture can be measured in vivo. One recently developed instrument which may have this capability is a dedicated X-ray based transaxial scanner constructed for measurements at the distal radius (the Stratec pQCT scanner). This instrument will be used to obtain an image of an excised femoral head. An initial assessment of the clinical usefullness of the instrument will be made, an important step towards developing an in-vivo method of quantitative structural analysis.

Chapter 2
Bone Structure and the Effects of Osteoporosis

2.1 An Introduction to Bone

Bone, on a macroscopic scale, is organized into two types: trabecular (spongy) and cortical (dense). The location and distribution of these two types of mineralized collagen are shown for the femur in figure 2.1.

Cortical bone forms the shafts of long bones and the external surfaces of all bones. It is composed of many different cylinders (Haversian systems or osteons) as illustrated in figure 2.2. "Osteon" is defined as the region of mineral-collagen matrix bounded by a Haversian canal on the inside and by a line called a cement line on the outside. Materials necessary for bone resorption and apposition within each osteon are transported in the canals. The spaces between the osteons are filled with lamellar bone, which consists of osteocytes distributed throughout the mineral matrix. The osteocytes communicate through a number of small canals called canaliculi. The space in the collagen-mineral matrix in which the osteocyte sits is referred to as a lacuna.

Despite the fact that eighty percent of the skeletal mass consists of cortical bone, in this study we will consider trabecular bone.

Figure 2.1
The Anatomy of a Long Bone

Showing Locations of Trabecular and Cortical Bone

From "The Anatomy Coloring Book"

a. epiphysis
a[1]: epiphyseal line
b. diaphysis (shaft)
c. articular cartilage
d. periosteum
e. trabecular bone and red marrow
f. cortical (compact) bone
g. medullary cavity and yellow marrow
h. nutrient artery

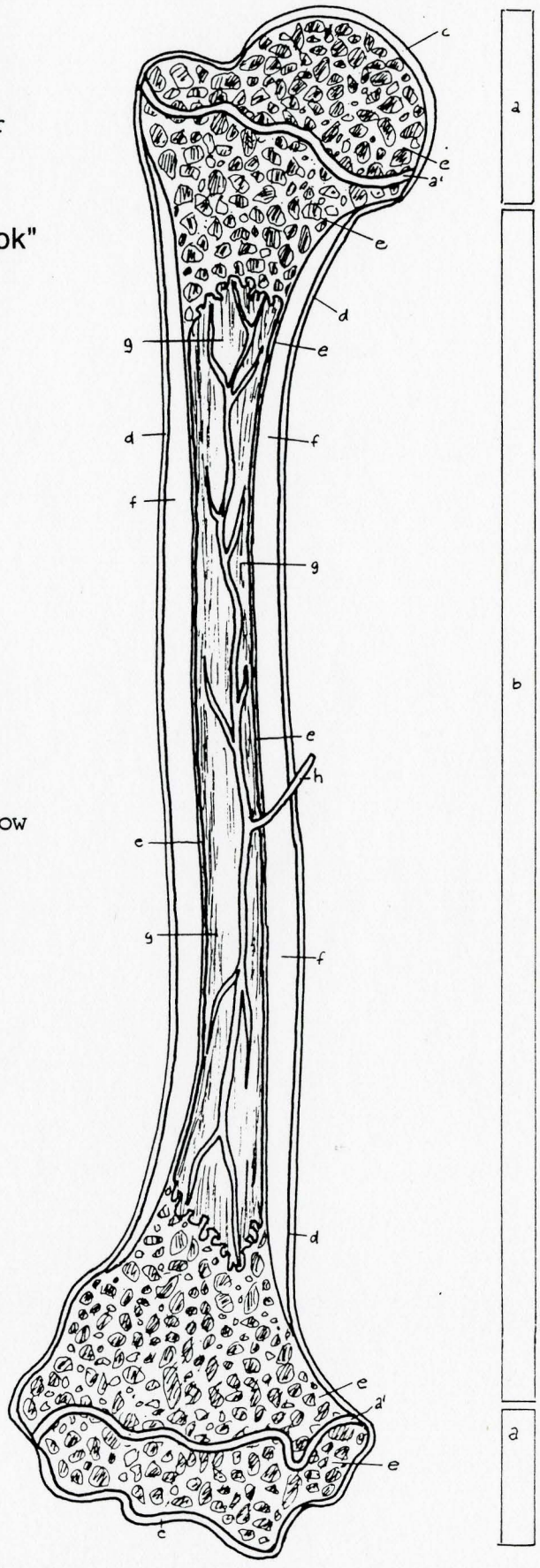

Figure 2.2
Cross and Longitudinal Section
of a Bone (rib)

Structural Units and Active Remodeling Sites

taken from Jaworsky

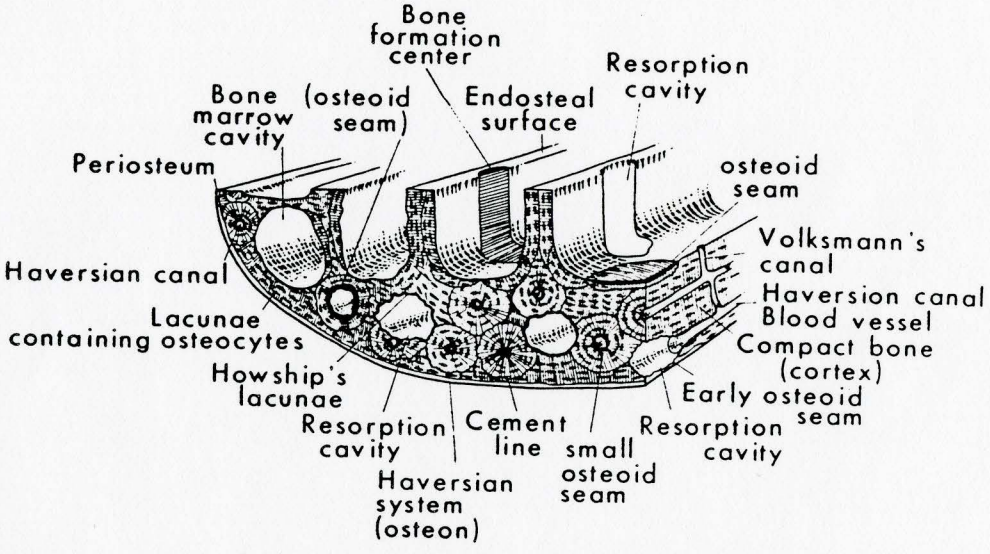

Trabecular bone is significant to the understanding of osteoporosis. Trabecular bone contributes to the strength of bone at common fracture loci (ie: vertebral bodies or the proximal femur), so its breakdown will result in weaker, more fracture-prone bones. Also, changes in bone metabolism will be manifested first in trabecular bone since turnover rates are three times higher in trabecular than in cortical bone [19] . Thus the important clinical consequences of osteoporosis are first evident at bone sites with a significant fraction of trabecular bone. It is for this reason that normal diagnostic methods measure bone mass in areas with a high percentage of cancellous bone (ie: proximal femur, vertebral bodies).

Trabecular bone exists at the ends of the long bones such as the proximal femur, in the vertebral bodies, and in the majority of the flat bones. As shown in figure 2.1, long bones are divided into distinct regions by a cartilaginous plate (the metaphysis), which occurs near the ends of the bone. It separates the ends or tips of the bones (the epiphyses) from the middle portion of the bone (the diaphysis). The metaphyseal plate normally disappears after maturity. Bone epiphyses are trabecular bone with a cortical shell, while the diaphysis consists of a hollow shaft of cortical bone with trabecular bone at its ends. This shaft, as well as the spaces within the trabecular bone, is filled with bone marrow.

Haversian systems in cortical bone arise from remodeling of lamellar bone by osteoclasts and osteoblasts (section 2.2). In trabecular bone, bone remodeling takes place directly on the surface of the plates (trabeculae) of the 3 dimensional web. The total area for formation and resorption in trabecular bone in the skeleton is about 10 m^2, about three times the value for cortical bone [19]. This is part of the reason why changes in remodeling activity manifest themselves first in trabecular bone.

Trabecular spacings are from 0.5 to 1.0 mm while plate thicknesses range from .10 mm. up to .15 mm. These figures are for healthy bone [20]. Figure 2.3 shows trabecular networks in normal and osteoporotic bone. Compare the relatively thick plates and small inter-plate spacings in the normal bone with their counterparts in the "corroded" osteoporotic network. During osteoporosis, trabeculae are eliminated by resorption and not replaced. This process is an irreversible architectural change. In some osteopenic processes the trabeculae become thinner through mineral loss but do not disappear. This type of architectural change is reversible.

2.2 Growth, Modelling, Repair and Remodeling

Bones are by no means static organs. Obvious dynamic processes are growth and repair in the event of an injury. Healthy bone also constantly undergoes a process called remodeling. Growth in length of a bone occurs by endochondral ossification [21 pg 7]. Growth in diameter occurs by deposition of new bone onto the existing periosteal bone surface. The endosteal surface of the bone is at the junction between mineral and marrow.

Modelling is defined as a process whereby bones maintain their shape during the period of growth. If a bone increases its length through growth, then the mineral distribution is altered by modelling so that the bone retains its shape. Remodeling is the process in which bone mineral is constantly being removed (resorbed) and reformed (apposited) even in individuals in whom no growth or macroscopic change in the bone is taking place. The purpose of remodeling is to allow bone to constantly adapt to

Figure 2.3
Trabecular Networks in Healthy and Osteoporotic Bone
Magnification X14.5
Maceration preparation
Electron Micrograph
Taken from Sandoz Publication [20]

a: Healthy Bone

b: Osteoporotic Bone

mechanical stresses and to repair microfractures which result from these stresses. Although the shape of the bone does not change, the trabecular architecture may, which is why this process is of concern to us.

In both cortical and trabecular bone, mineral is constantly being resorbed and apposited. Differences in these two rates can cause a net loss or gain of bone mass. The rates can be affected by various biochemical and mechanical factors in both normal subjects and in patients suffering from a range of diseases. Simplifying the hormonal picture, parathyroid hormone stimulates resorption while calcitonin suppresses resorption. The hormonal picture is actually incredibly complex. Other hormones, all of which have a hand in the regulation of resorption and formation of bone, are vitamin D, thyroxine, insulin, growth hormone, testosterone, estrogen and cortisol. There are also bone growth factors which can exert local influences over the rate of bone turnover. Thus there exists an extensive variety of biochemical means of manipulating bone cell metabolism. Other factors such as mechanical stress, physical trauma, or electric fields can affect the rates at which these various processes occur.

The osteogenic cells which are under the control of these hormones and growth factors are

1) The osteoblast which lays down bone matrix;
2) The osteoclast which resorbs bone and
3) The osteocyte which has a controversial function involved in blood-bone mineral exchanges.

The rate of bone turnover is estimated to be 3 to ten times higher in trabecular than in cortical bone. The presently accepted

ICRP rates are 2.5% and 10% (of existing bone mass) per year for cortical and trabecular bone respectively.

2.3 Mineral Exchange Locations

Mineral exchange, resorption and apposition must necessarily take place at bone surfaces. Thus, this is where we find the osteoclasts and osteoblasts, and it is these surfaces that are the areas of bone sensitive to radiation damage. The most obvious surface of bone is the periosteal, or outside surface. Other surfaces are the endosteal surface (lining the marrow cavities, just inside the outer cortical shell) and the sides of the haversian canals. Trabecular bone has a very large amount of surface area due to the nature of the trabeculae. In lamellar bone, the surfaces are at the margins of the bone and along the canaliculi.

2.4 Crystal Structure

On the scale of angstrom to micron, the structure of bone is less well understood [22]. The basic building blocks are plate-shaped crystals of hydroxy apatite ($Ca_5(PO_4)_3OH$ -- referred to as dahlite). The other building blocks are collagen fibrils, which link to create "frames" on which the mineral crystals deposit. The crystals are a few hundred angstroms long and a few tens of angstroms thick. The size of these crystals seems to increase with age of the organism until maturity, at which time it reaches a plateau [23].

The basic building block of the collagenous framework is the

"triple helical molecule." These are arranged in staggered arrays, with channels produced by the staggering. It is believed that most of the crystals fit into these channels. The remaining crystals attach outside the fibril.

Bone generally is composed of lamellae of mineralized collagen fibrils. The fibrils within a lamellae are arranged in roughly parallel layers. Orientation of fibrils in alternate lamellae vary, in the same way that grains in alternate layers of plywood are varied to produce a structure of maximum strength. The plywood structure is due to the offset in orientation of collagen fibrils in adjacent lamellae as well as to the rotation of individual fibrils around their own axes.

2.5 Impact of Osteoporosis on Bone Structure

Osteoporosis affects mainly the endosteal bone surfaces (cortical and trabecular) and the inner third of the cortex of the long bones. Thus osteoporosis in adults is characterized morphologically by a thinning of the cortex, an expansion of the medullary canal (marrow cavity), and a thinning and loss of the trabeculae [24 pg 487].

Chapter 3
Materials and Methods

3.1 Bone Samples

Proximal femur samples were obtained from hip replacement surgery through the pathology departments of the participating hospitals. The samples were of varying size, depending on the position of the break. Usually the whole femoral head was recovered, with varying extents of the femoral neck as illustrated in figure 3.1. The samples were received in formalin-filled buckets (those from McMaster University Medical Centre), or in plastic bags containing a small amount of formalin (those from Hotel Dieu Hospital, St Catherine's). Twenty-four whole femoral heads were obtained for the actual study. A number more were used for preliminary experiments.

To facilitate later cutting, the samples were baked in a small oven to remove the marrow. To leave the mineral intact, the baking was done at a low temperature (110 C). Baking time was 14 hours.

For some preliminary work, since it was difficult to obtain a sufficient number of samples through the hospitals, a number of

Figure 3.1
Right Femur, Anterior Surface

Taken from C.P. Anthony, N.J. Kolthoff, Textbook of anatomy and physiology, 9th ed., St. Louis, U.S.A., The C.V. Mosby Company.

complete femurs were obtained from a commercial supplier[1]. These were already dry. Because of the unknown preparation method, quantitative values from these samples were not comparable to the samples obtained from surgery. However, they were useful in establishing methods and trends which would apply to the other group.

3.2 Slicing of Femoral Heads

For purchased femurs only, the head was removed from the main shaft by slicing at the femoral neck with a bandsaw. The cut was made in the middle of the femoral neck through a plane perpendicular to the axis of the neck. Samples obtained from surgery were already broken from the rest of the femur.

A low speed saw[2] was used to obtain the thin slice of bone from the head. It was necessary to notch the femoral head for it to fit one of the chucks supplied with the circular saw which is shown in figure 3.2. The notch was cut on the side of the femoral head in such a way that when held by the notch, the bone was positioned properly to take a slice from a vertical plane running through the long axis of the femoral neck. The blade was positioned

---

[1] Osta International
922 Keil St.
White Rock, B.C.
V4B 4V7

[2] 11-1180 Isomet Low Speed Saw, manufactured by
Buehler International
41 Waukegan Road
Lake Bluff, Illinois
60044 U.S.A.

in Canada

Tech-Met Canada Ltd.
9999 Highway #48
Markham, Ont.
L3P 3J3

Figure 3.2

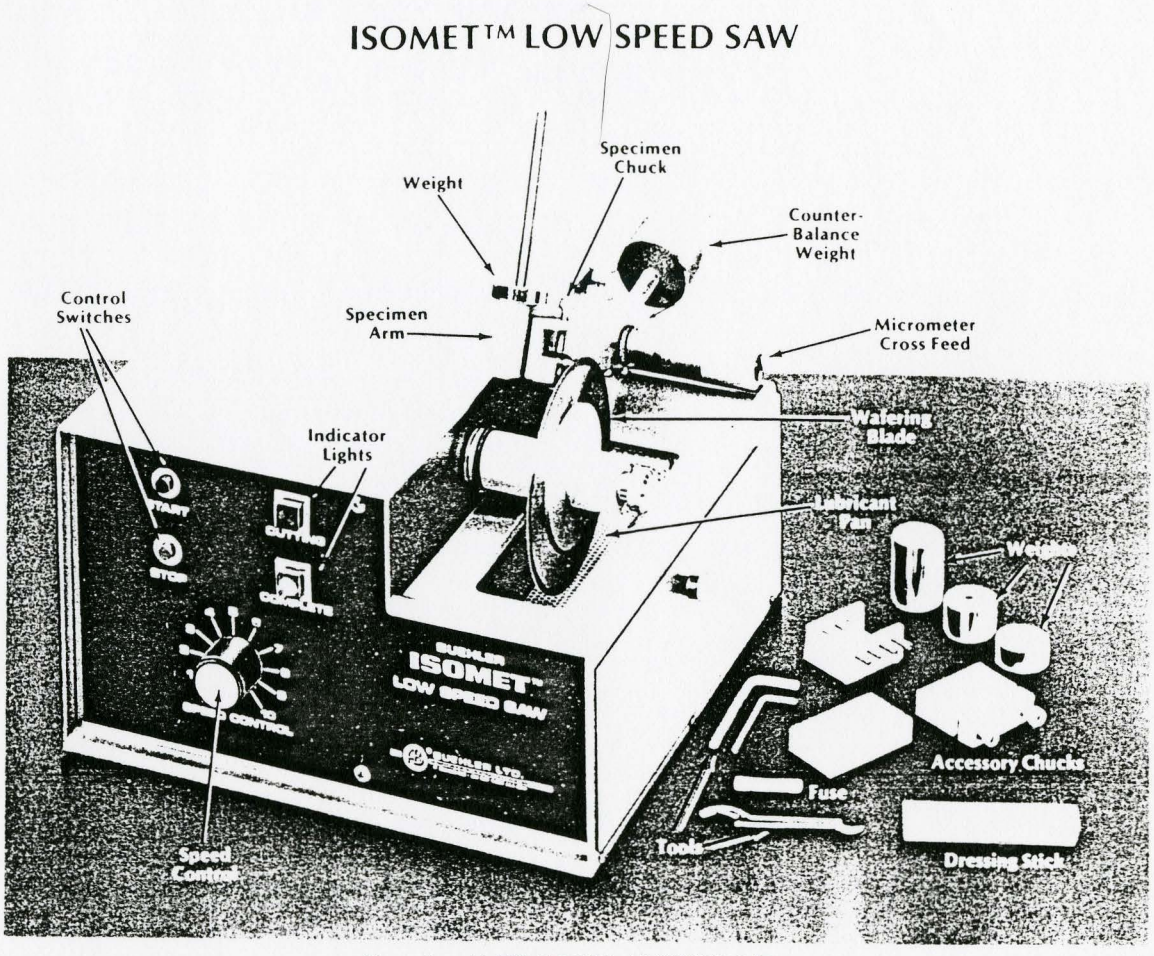

Figure 1. — 11-1180 ISOMET™ LOW SPEED SAW
(with Standard Accessories)

approximately at the centre of the head for the first cut. The position of the micrometer blade was noted and the cut made. Since the radius of the blade was not enough to remove the section, it was necessary to turn the sample 180 degrees to finish the cut. This was accomplished simply by loosening the chuck mount bolt and rotating. In this manner, the first cut was completed, allowing the half of the femur not held by the chuck to fall away. The bone was shifted 3.5 mm using the micrometer, and a second parallel cut made in the same manner to give a 3.5 mm thick cross-section of bone. Figure 3.3 shows the positions of the cores and the 1 cm slabs from which they were taken, as well as the position of the thin X-ray slice.

3.3 Taking the X-ray

A contact X-ray was taken by placing the cut section on high-resolution film[3] in a Faxitron model 805 x-ray machine[4]. Trial and error showed the best resolution was given using 50 kVp for 30 seconds. Standard processing was done using the Kodak processor located in the Dept. of Nuclear Medicine, MUMC.

---

[3] Kodak EctaScan Type B EB-1 Cat. #1981810
Eastman Kodak Company
Rochester, N.Y. 14650
U.S.A.

[4] Faxitron 805 Radiographic Inspection System
Field Emission Corporation
Melrose Avenue at Linke Street
McMinnville, Oregon, U.S.A. 97128

Figure 3.3

Position and Orientation of Slices/Cores

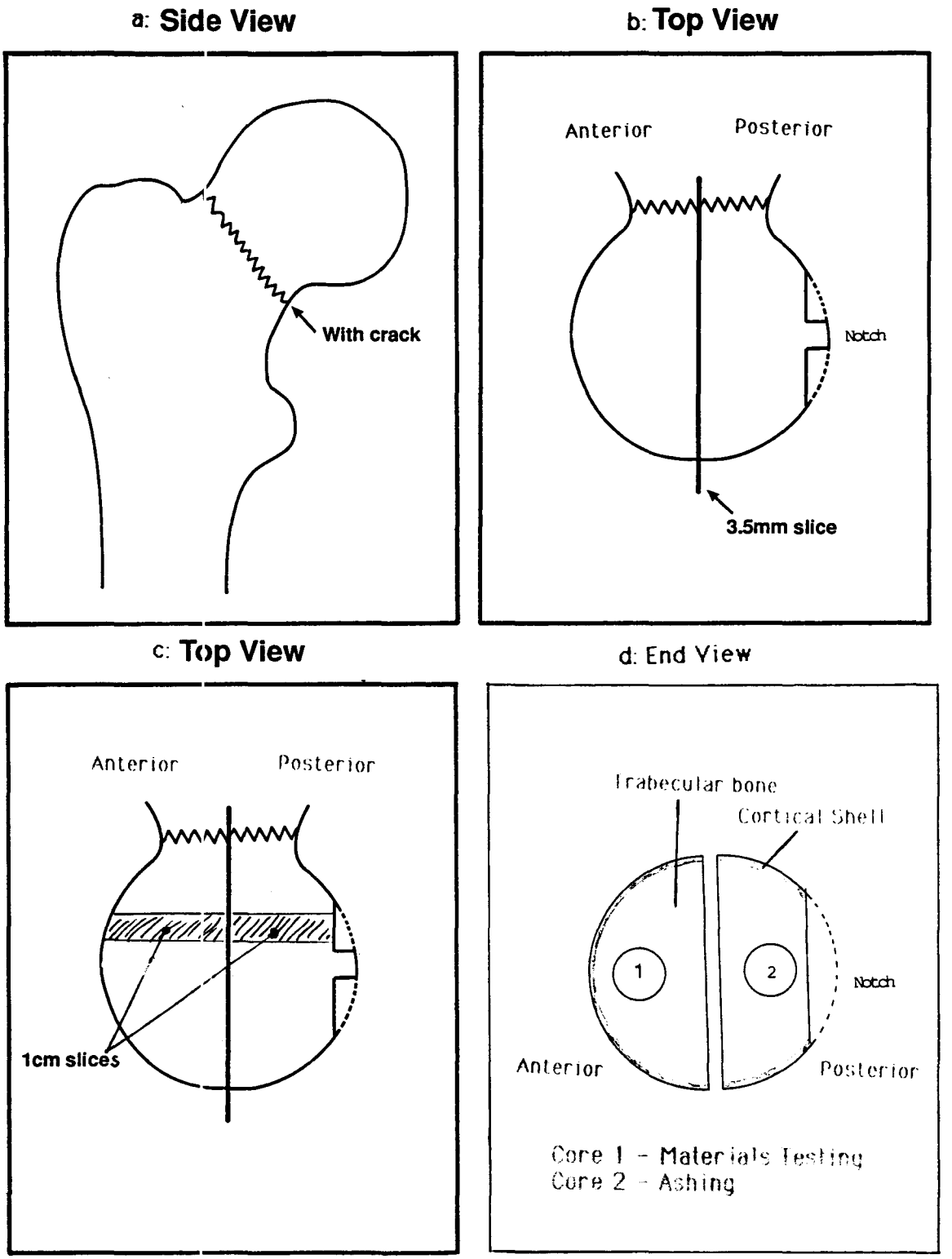

3.4 Obtaining Cores for Crushing or Ashing

A coring drill bit of 1.25 cm (1/2 inch) bore satisfied the constraints of being large enough to obtain a core of measurable value on the materials testing machine while being small enough to obtain several cores from one femoral head when necessary.

A slab of bone from which the core was taken was removed from the femoral head by making two parallel cuts 1 cm apart (using the Isomet saw as in section 3.2). The cuts were made perpendicular to the axis of the femoral neck. The core was taken through the cut ends of the slab (in the direction of weight-bearing). This gave a core of one centimetre in length and 1.25 cm diameter with parallel end faces. The latter condition is necessary for proper testing in the hydraulic press (section 3.6). Cores of trabecular (as opposed to cortical) bone were taken. The location of the core and the slice it was taken from is shown in figure 3.3.

3.5 Ashing a Core

The length of the core was measured with vernier calipers. Core lengths ranged from .98-1.01 cm, confirming that the micrometer arrangement on the Isomet saw was accurate. Nevertheless, the length of each core was measured and the caliper reading used as the "true" value rather than assuming all to be exactly 1 cm long. The calipers were again used to confirm the core diameter to be the 1.25 cm bore diameter of the drill bit. This dimension was found to be accurate within .005 mm in all cases, so 1.25 cm was used as the "true" value. Knowing the dimensions of the core, its volume could be calculated. The core was weighed. This is the wet weight of the bone sample.

The core was ashed in a nickel crucible in a muffle furnace for 48 hours. The first 24 hours were at 475°C, the second 24 hours at 650°C. This should have been enough time to assure that the samples were completely ashed. At the end of the ashing period, the oven was turned off and opened, and the samples allowed to cool for one hour in the oven. This period of cooling was sufficient so that the samples could be handled. The samples were then allowed to cool outside the oven for an additional 15 min. This lag time assured that the crucibles regained any adhering water they might have lost. This allowed us to safely assume the change in weight measured was due to changes in the bone rather than to changes in the crucible.

At the end of the final 15 minute cooling, the samples were weighed. Subtracting the weight of the empty crucible from the final gross weight gave the final weight of the bone ash. The ash weight over the originally measured volume of the sample was the ash density of the core (calculated in g/cm^3).

3.6 Determining the Failing Strength of a Core

A core from a standard position/orientation in the femoral head was crushed using a Lloyd's material testing instrument[5].

The Lloyd's machine is a computer-linked hydraulic press. The sample is placed in the press, and the sample compressed at a preset

[5] Lloyd Instruments Ltd.
7 Whittle Ave.
Segensworth West
Fareham Hants
PO15 5SH England

in Canada: Omnitronix
#1-2180 Dunwin Drive
Mississauga, Ont.
L5L 1C7

rate (set in mm/s). The force exerted by the press is measured by the system and plotted against the deflection. As the sample is compressed more and more the force builds up, until the point at which the core fails. At the point of failure, the compressive force exerted by the press is a maximum. This value is referred to as the maximum compressive strength. Figure 3.4 shows the results of a typical run on the Lloyd's press. In this case the maximum compressive strength was 1120 N.

It is important for the sample being measured to have plano-parallel ends. This ensures that the sample is subjected to compressive forces only and not shear forces. This condition was met by preparing the samples as discussed in section 3.4.

As there is evidence that measured maximum load strength depends on the rate of compression [25], this rate was standardized at .5 mm/min for all tests.

The failure load for compression, tension, or shear force is given by

$$L_f = A\sigma_f \qquad (3.1)$$

Where L_f is the failure load, σ_f is the material strength (the sample-specific property we are trying to compare), and A is the cross sectional area of the sample [26]. Since we have standardized A by using cores of the same size, L_f is a function of σ_f only. The failure load should not theoretically be dependent on the length of the sample, but this parameter was standardized as well.

Other information is available from the graph in figure 3.4. Young's modulus is defined as

$$Y = \frac{\frac{F}{A}}{\frac{\Delta L}{L_0}} = \frac{\text{stress}}{\text{strain}} \qquad (3.2)$$

Figure 3.4
Typical Output From Materials Testing Machine

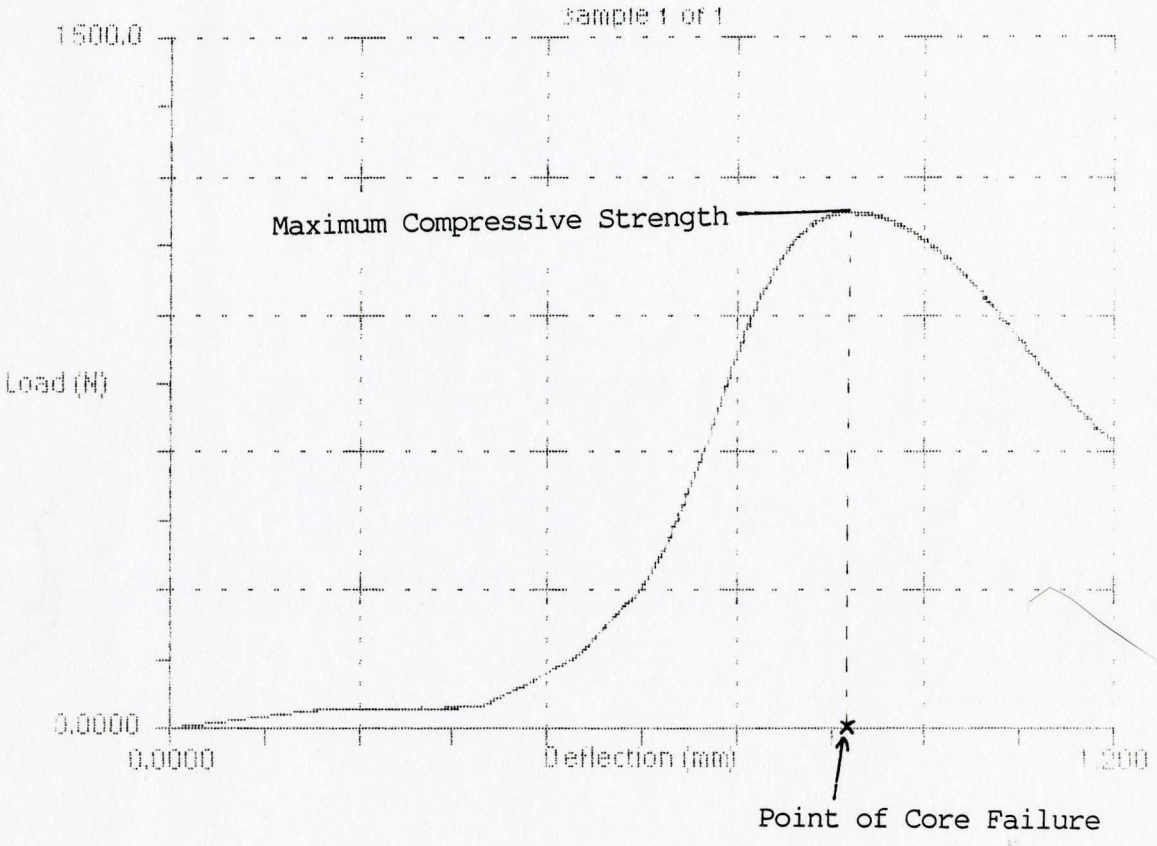

where F is the applied force, A is the cross-sectional area of the sample, ΔL is the change in length of the sample, and L_0 is the original (undeformed) sample length. Since the slope of the crushing curve is $F/\Delta L$, Young's modulus is obtained by multiplying it by a factor L_0/A. The slope used to calculate Young's modulus is from the linear part of the buildup phase of the crushing curve.

Another variable that can be determined from the compression curve is "work to failure", which is the integral of the load-compression curve. This integral is the area under the curve up to the point of failure.

The three variables discussed above, maximum compressive strength, Young's modulus, and work to failure, were determined for each bone. All 3 were analyzed for their correlations with ash density and connectivity since it was unknown which best represented bone strength in the sense of resistance to fracture.

3.7 Quantitative Trabecular Analysis of X-rays

The final goal of obtaining a high-resolution x-ray of a thin slice of femoral head was to quantitatively analyze the trabecular structure. This analysis was done on an existing system at MUMC[6]. There are many parameters of a trabecular network that could be quantitated. Mean thickness or length of trabeculae, directionality of the system, mean spacing between trabeculae, as well as more complicated secondary parameters could all be analyzed. Dr. Arsenault's system was originally set up to quantify the number of nodes, or points where trabeculae connect, in a

[6] The image analysis system used was put together by Dr. L. Arsenault in the Electron Microscopy Department.

trabecular network. Since this variable has been used by previous architectural researchers [27, 28, 29], it was used in this study. The femoral heads used varied in size and it was necessary to normalize for the area of the image. Therefore the quantitative value used is not simply the number of nodes, but the number of nodes per unit area. Area was measured in pixels. Only relative and not absolute values were needed. Since all images were analyzed under the same magnification it was unnecessary to convert pixels to a metric value. Under the magnification used in this project, there were approximately 12 pixels per square mm.

Chapter 4
Preliminary Experiments

To have confidence in the measured ash weight of a core, the effects of several variables had to be determined:

1) Does the container (nickel crucible) change weight during the ashing process? If this change is more than a few percent of the change in weight of the bone itself, it will have to be taken into account.

2) How long must the samples be baked to burn off all the marrow?

3) How much does bone density vary through the femoral head? How critical is standardization of positioning of the cores?

Questions 1 and 2 are addressed in section 4.1. Question 3 is addressed during preliminary strength testing work in section 4.2.

4.1 Ashing of Cores

It was thought that the crucibles may change weight during the ashing process. Small amounts of water, dust particles, or skin oil from handling could be removed during ashing. The ash weight of the samples was measured inside the crucibles. Thus a change in crucible weight could cause errors in measured ash weight.

To determine the weight change of the crucibles during the heating process, they were heated empty at the same temperatures and for the same time as for ashing samples. The initial weight of the crucible was compared to its weight immediately after the end of the heating period. This procedure was repeated twice on a set of two crucibles. This data is shown in table 4.1a. In both trials, the crucibles were weighed ten minutes after the oven was turned off at the end of the ashing period. It was necessary to wait ten minutes in order to allow the crucibles to cool enough to be handled safely. In trial 1, the crucibles were allowed to cool in an unopened oven. In trial 2, the oven was opened immediately when it was turned off to allow a more rapid cooling. This difference is evidenced by the measured weight loss in trial 2 being much lower than in trial 1. This is due to the crucibles in trial 2 cooling more, and thus regaining much of the water, and thus original weight, that they had lost.

To know if the weight loss of the crucible is significant relative to our measured value (ash weight), we must know a typical ash weight. To calculate this, the crucibles were heated again, this time with a sample inside. It was assumed that the crucible did not change weight (this error was ignored for the time being). The sample weight was calculated from the gross weight by subtracting the initially-measured weight of the crucible. Again, weighings were done 10 minutes after the end of the ashing period to allow for safe handling. Three trials were done, each time using two samples. This information is presented in table 4.1b.

Table 4.1 shows that the smallest ash weights can be around 0.15g, and the largest changes in crucible weight around 0.05g. An error of this magnitude introduced by changes in crucible weight is unacceptable and must be lowered. Therefore we must address the

Table 4.1

a: Weight Change of Nickel Crucibles During Ashing Procedure
b: Weight Change of Bone Sample

4.1a:

	Crucible	Initial (g)	After heating (g)	Weight Loss (g)
Trial 1	1	36.6314	36.5750	.0564
	2	36.9772	36.9390	.0382
Trial 2	1	36.6323	36.6233	.0090
	2	36.9772	36.9672	.0100

4.1b:

	Sample	Initial (g)	After heating (g)	Ash % of Wet Weight
Trial 1	1	.3770	.2160	57.3
	2	.4760	.2660	55.9
Trial 2	1	.4295	.2649	61.7
	2	.3748	.2301	61.4
Trial 3	1	.2538	.1552	61.1
	2	.4325	.2707	62.6

question of how long the crucible must be cooled to regain its original weight.

The crucibles were again heated empty for the standard times and at the standard temperatures. The weights of the empty crucibles were measured every three minutes for approximately 1 hour after heating. Figure 4.1 shows how the crucibles regain their mass as a function of time. At the end of the hour, measuring was stopped because the weights seemed to have stabilized. To confirm this stability, the crucibles were weighed again 2 days later and found to weigh the same as at the end of the hour.

It was of interest to know how a sample would change weight during this cooling period. Thus, the procedure used to produce figure 4.1 was repeated, this time with samples in the crucibles. This information appears in figure 4.2. The results are similar, except that this time the weights were not quite stabilized after one hour. 48 hours later the samples had increased an additional .0010g from the last weighing.

This information indicates that a cooling period of one hour after ashing is sufficient to almost eliminate weighing errors due to crucible weight change. As long as the cooling time is standardized, further changes in sample weight will not affect the legitimacy of the results for use in relative comparisons.

To see if the samples were completely ashed, two trials were conducted in which the samples were baked a second time. If complete removal of all non-mineral material had occurred in the first baking, no further weight change should be seen the second time. The ash lost only 0.5% of its weight when heated a second time. Again, this is barely significant. In terms of affecting the legitimacy of the ash weights for relative comparisons, this is not an issue, as long as the first ashing has been properly standardized.

Figure 4.1

Weight Change of Crucibles With Time
During Cooling Period

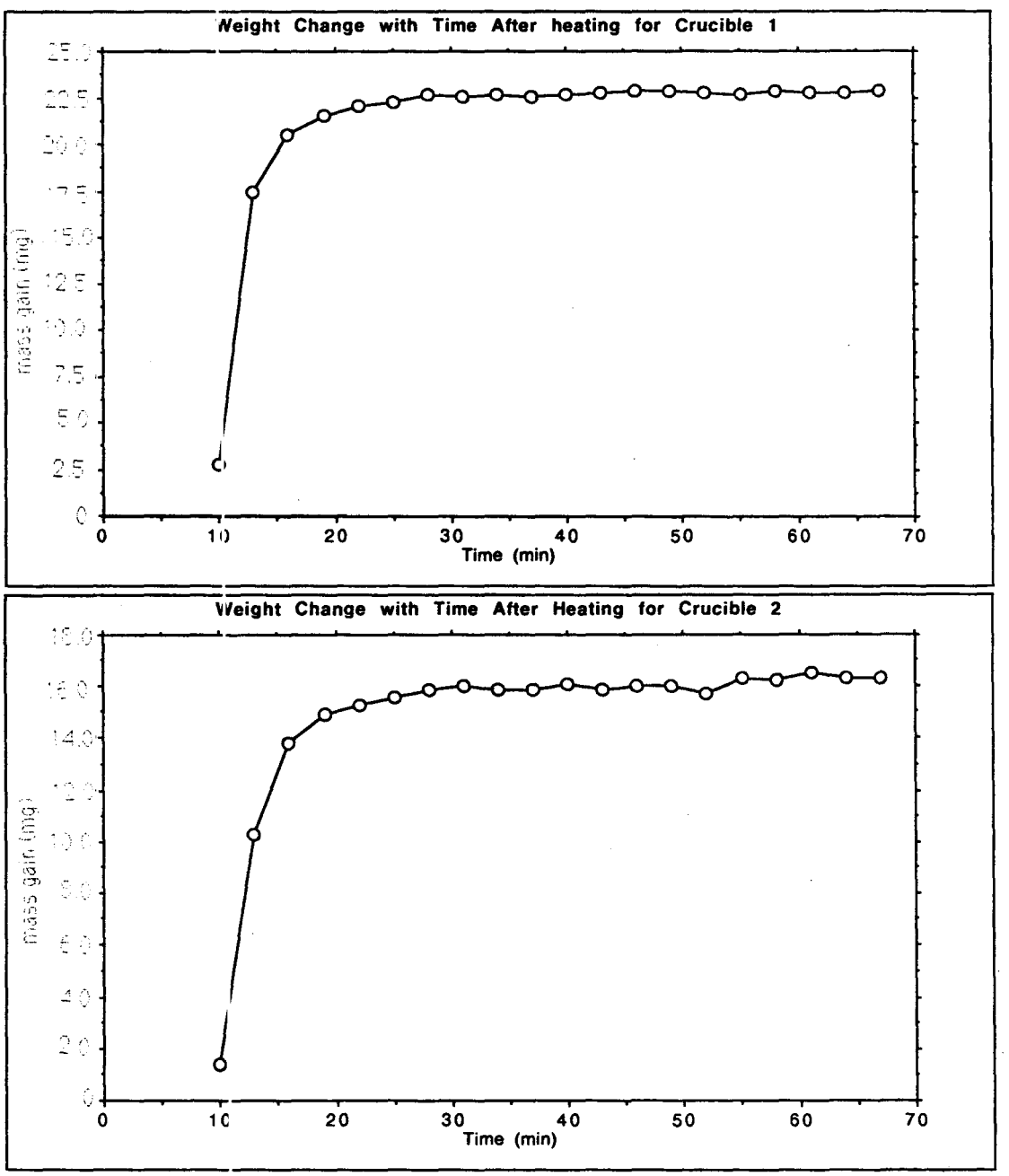

Figure 4.2

Weight Change of Crucibles and Samples
With Time During Cooling Period

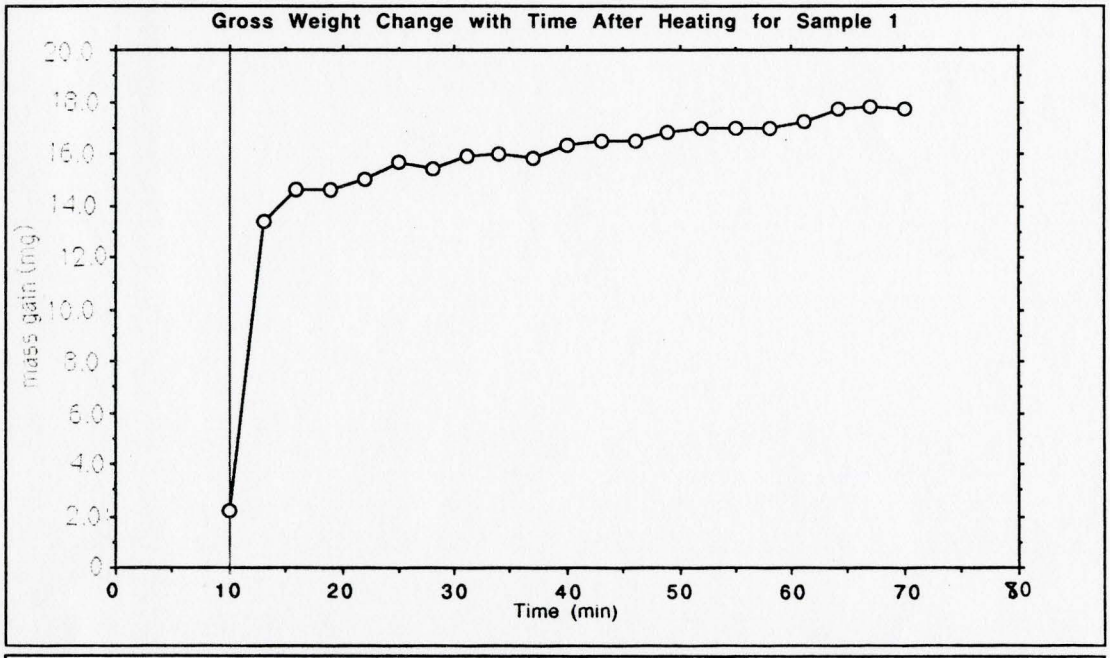

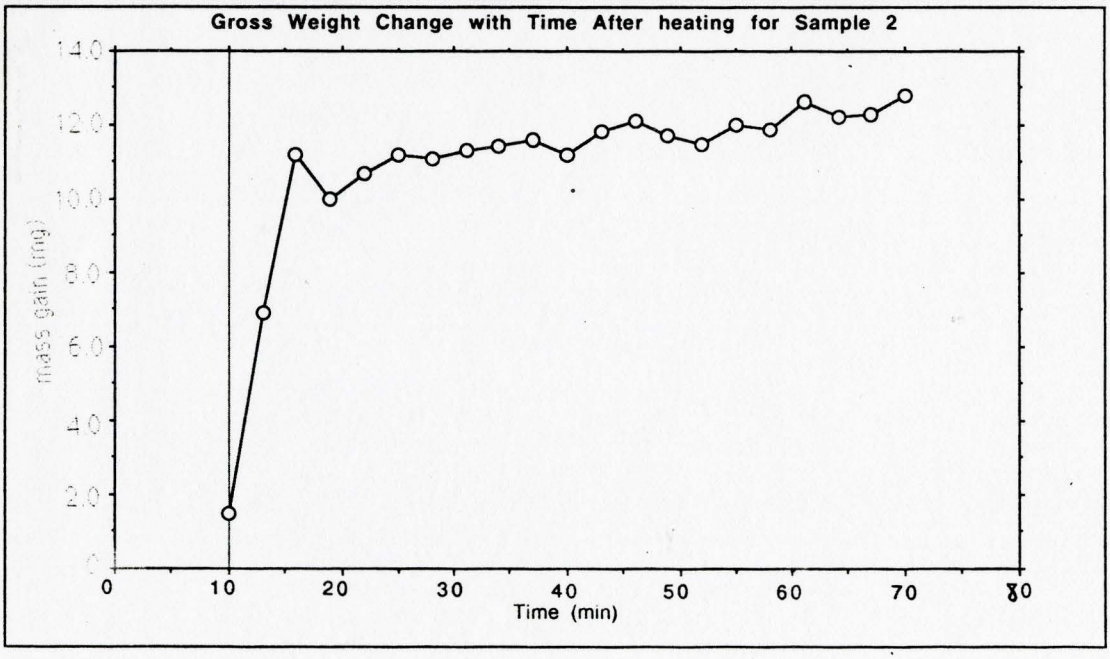

4.2: Measuring the Crushing Curve

To legitimize this quantitative comparison, it must be determined whether the crushing strength of one small core can be a representative value for the whole femoral head. Therefore we must find out how crushing strength varies with position in the head, with the eventual goal of finding a position suitable for a "standard" core. The strength of this core could be used to compare strength from sample to sample.

Thus a test was done using 5 (commercial) femoral heads. Four slices were taken from each head, each slice of approximately 1 cm in thickness. The slices were numbered from 1 nearest the tip of the femoral head to 4 nearest the femoral neck. The position and orientation of these slices is shown in figure 4.3. From each of these slices, a number of different cores were taken using the 1.25 cm bore drill bit. The position of each core is denoted using standard anatomical nomenclature[7]. Each core was weighed and its dimensions measured using vernier calipers. From this its density[8] was calculated. Then, each core was crushed to produce its crushing curve.

Using the densities, strengths, and positions of the cores, a crushing and density profile was determined for each femur. Figures 4.4 to 4.8 are the density profiles. Variation in dry bone density should be a reasonable approximation of variation of ash density, as

---

[7] Inferior/Medial/Superior refers to vertically varying positions in a standing subject. Ventral/Medial/Dorsal refers to horizontally varying positions (horizontally from back to front), again in a standing subject.

[8] Note that this is not an ash density, but rather the density of the dry bone of the commercial femur.

Figure 4.3
Position and Orientation of Slices
Used in Finding Density and Strength
Profiles

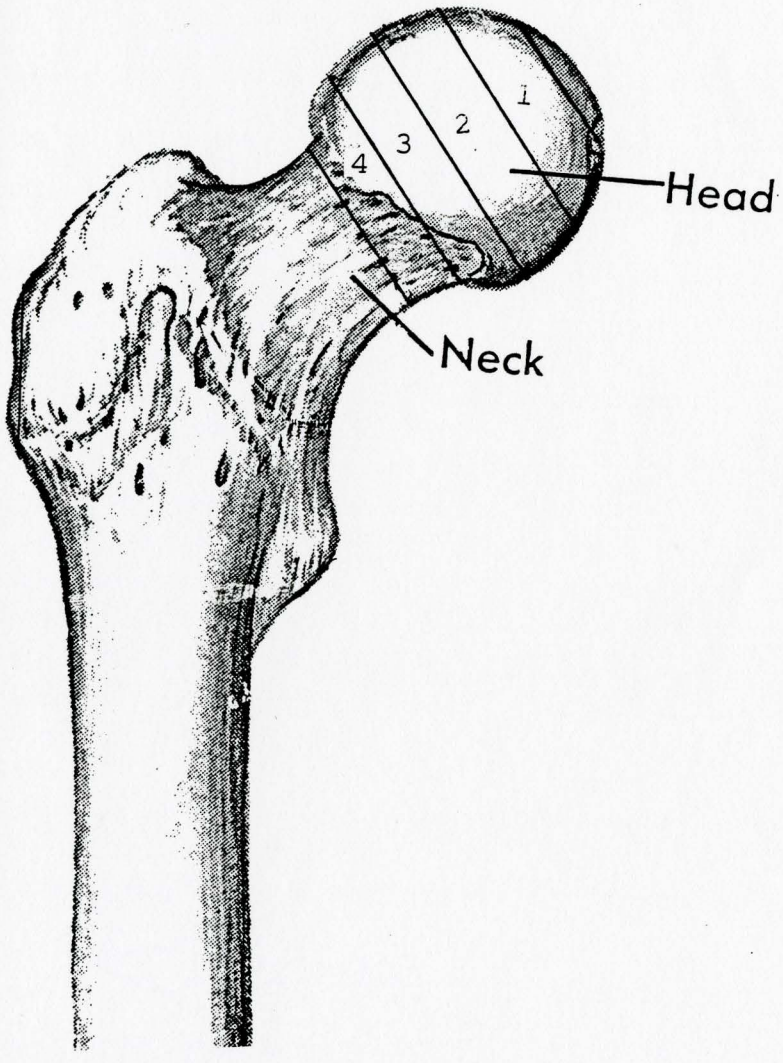

Figure 4.4

Density Profile for Femur 3

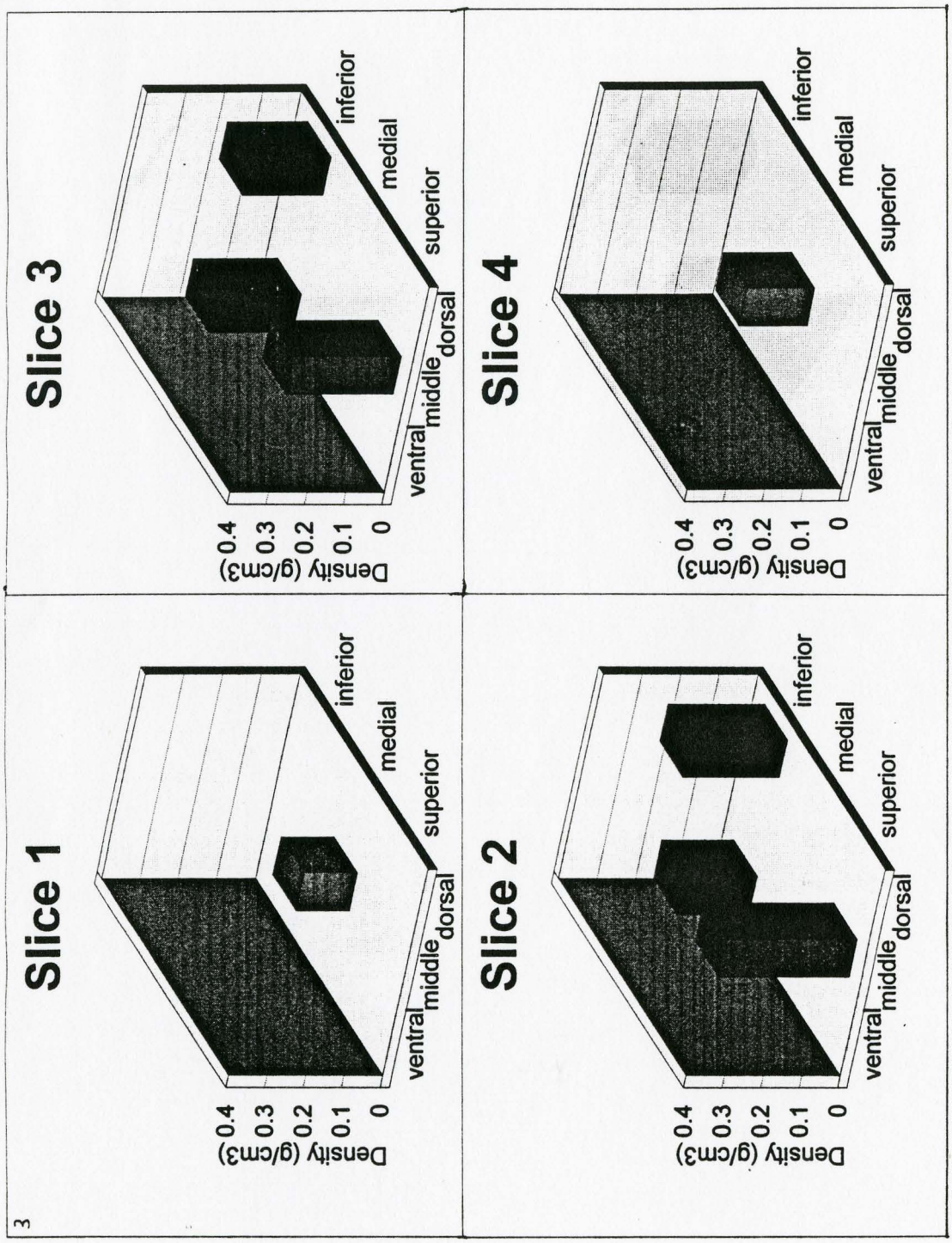

Figure 4.5

Density Profile for Femur 4

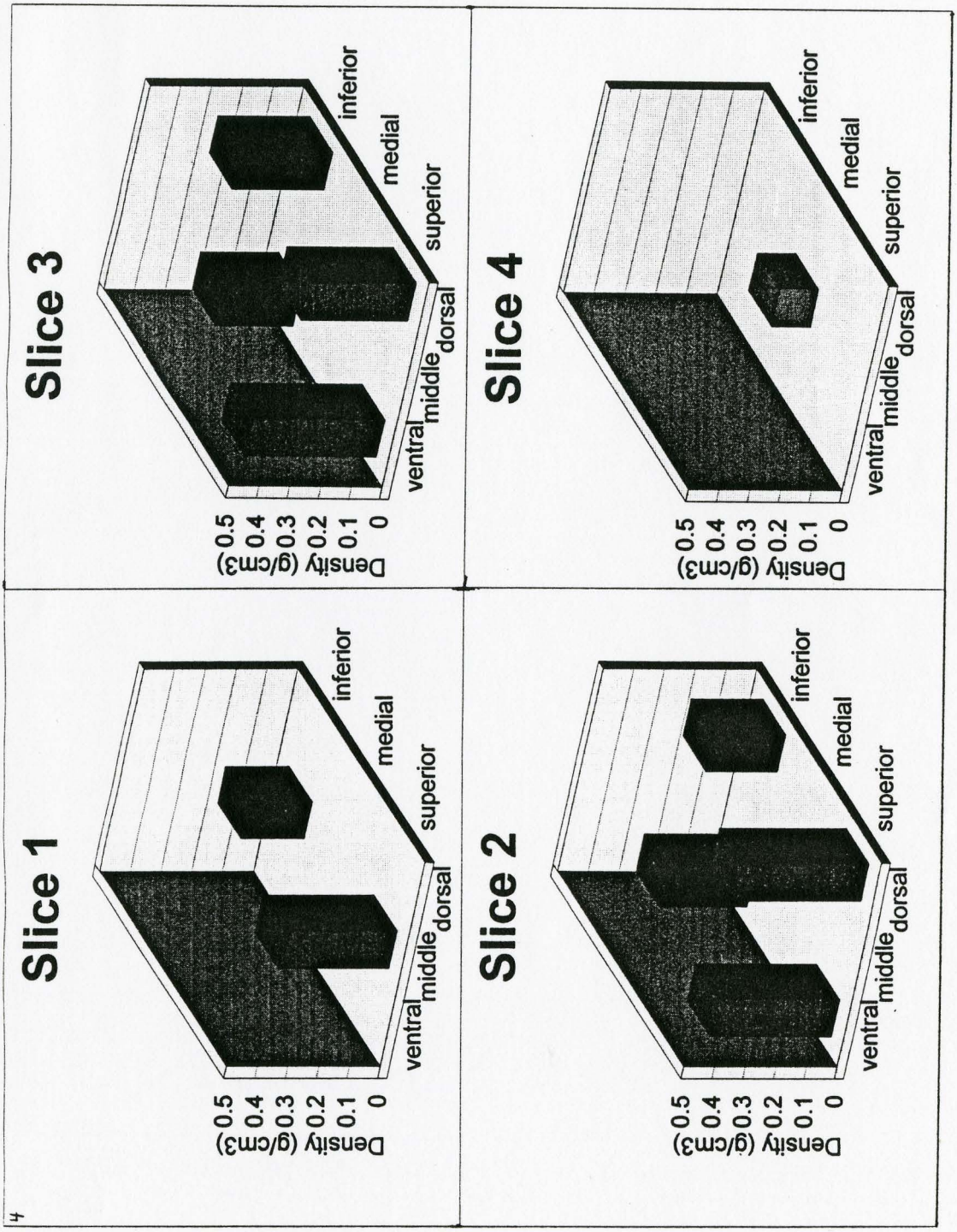

Figure 4.6
Density Profile for Femur 5

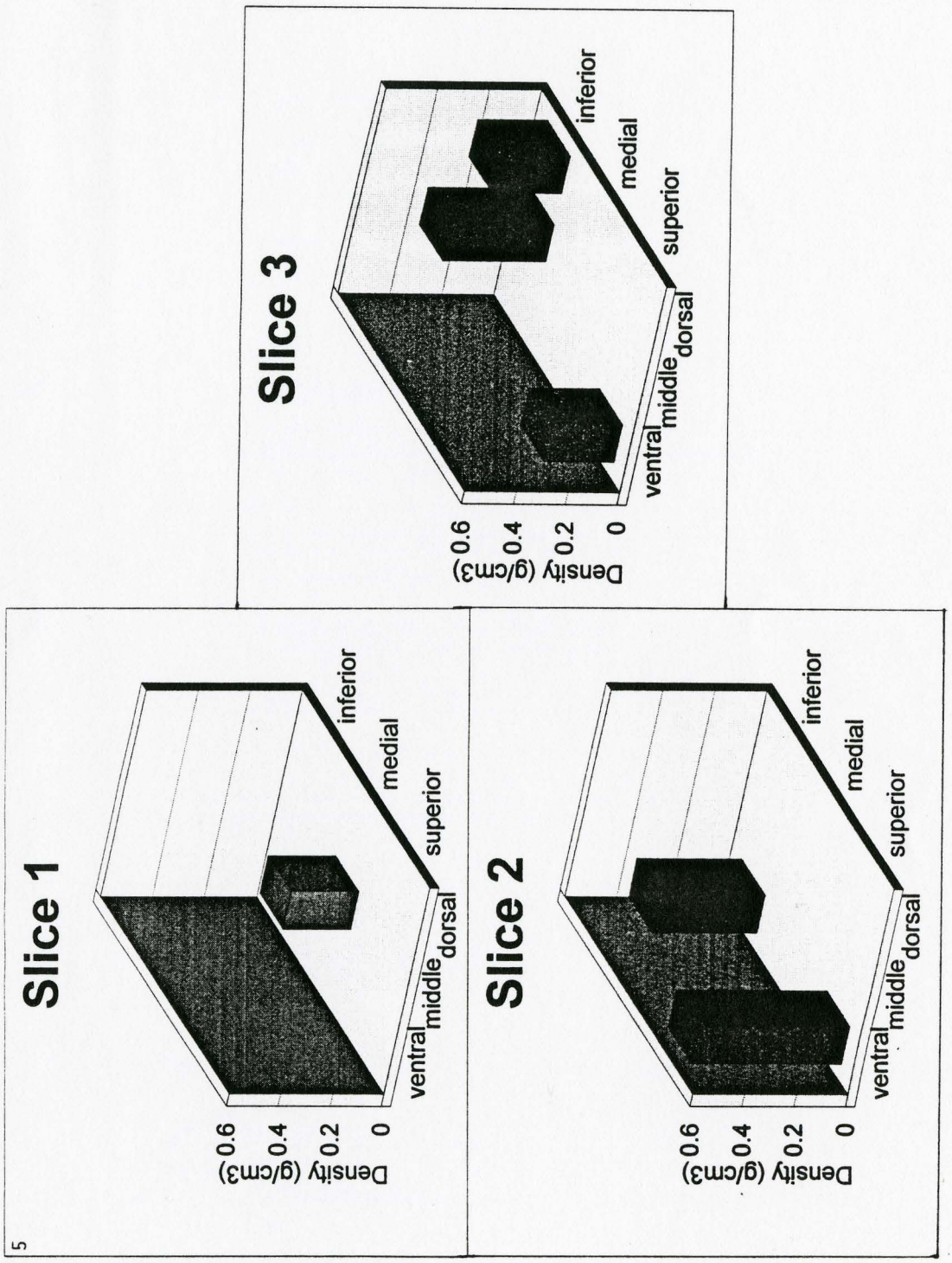

Figure 4.7
Density Profile for Femur 6

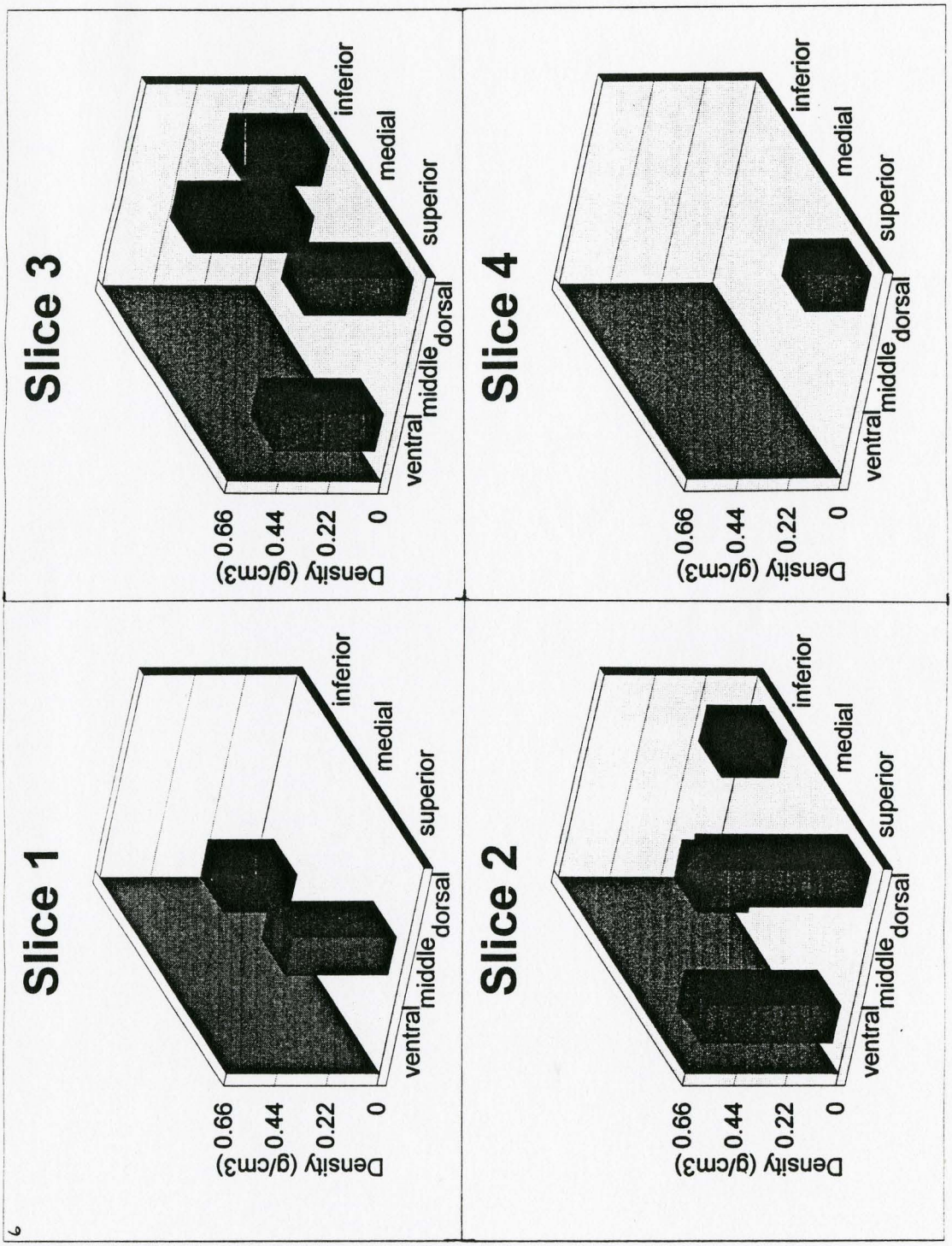

figure 4.8
Density Profile for Femur 7

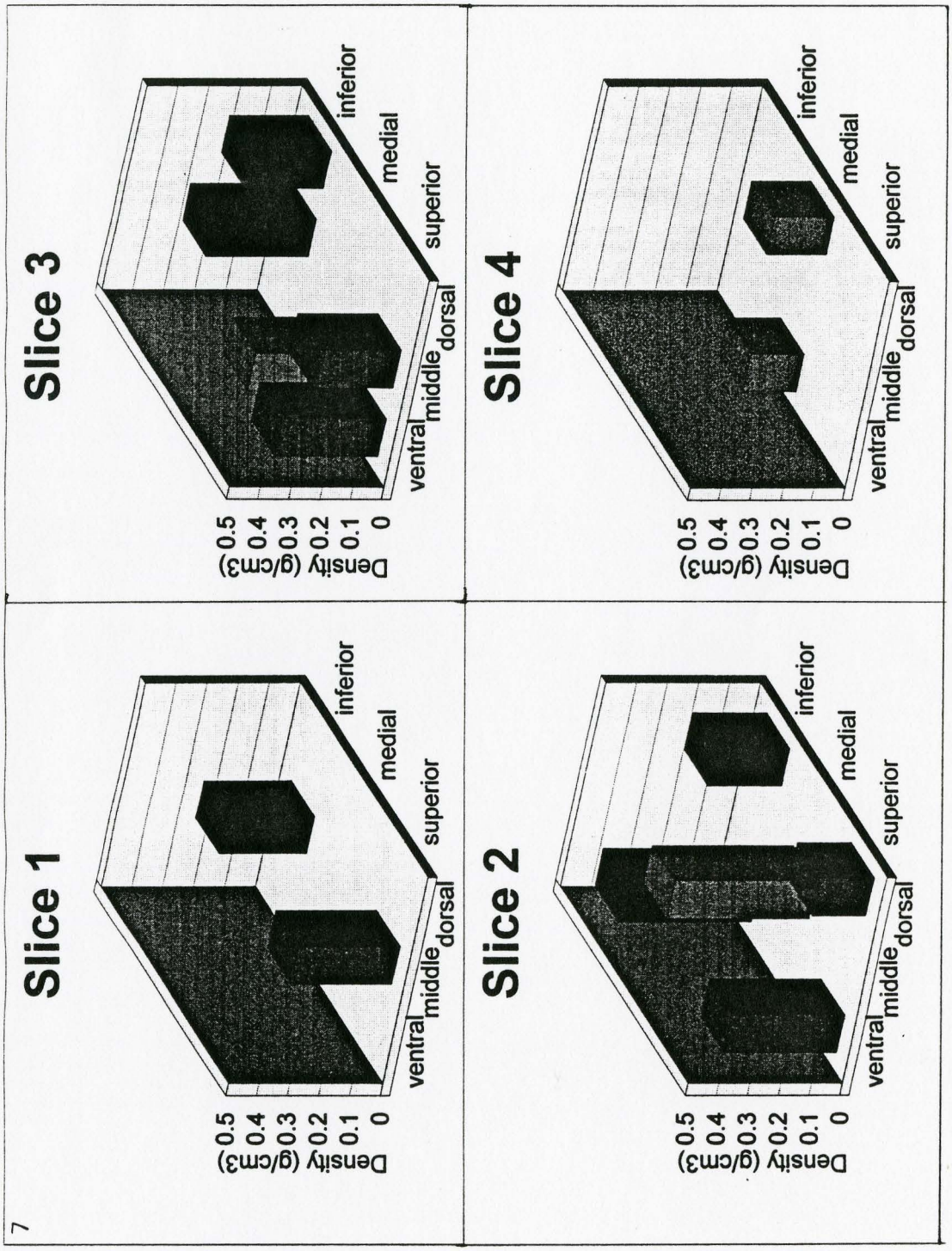

is evidenced by table 4.1b. Note that the ash % of dry bone is quite stable, varying less than 7%.

Figures 4.9 to 4.13 are the maximum compressive strength profiles. Work-to-failure and Young's modulus are so highly correlated to maximum compressive strength that their profiles should be analogous.

From the profiles, we can see that spatial variations in strength and dry bone density are not exactly the same from sample to sample. However, in every case slice 3 seems to give the most predictable values relative to other slices in the same sample. Therefore we used cores from slice 3 to give values for ash density and crushing strength representative of the sample from which they originate. For purposes of standardization, the core for crushing strength measurements was taken from the anterior part of the head and the core for ash density measurement from the posterior half in each case. Both samples were taken from a medial position in the vertical (superior-inferior) dimension.

4.3 Quantifying Architecture:

We are necessarily dealing with a two-dimensional projection (X-ray) of a three dimensional system (the trabecular network). To produce numerical results which can be compared relatively, a standard slice thickness was selected to eliminate errors due to projection effects (false nodes[9]). It must be emphasized that the results only have relative legitimacy. The numbers are not accurate in an absolute sense, as the effect of false nodes has been standardized rather than determined.

[9] False nodes are apparent cross-points resulting from two trabeculae, unconnected in 3-space, projecting onto one another in 2-space.

Figure 4.9
Crushing Strength Profile for Femur 3

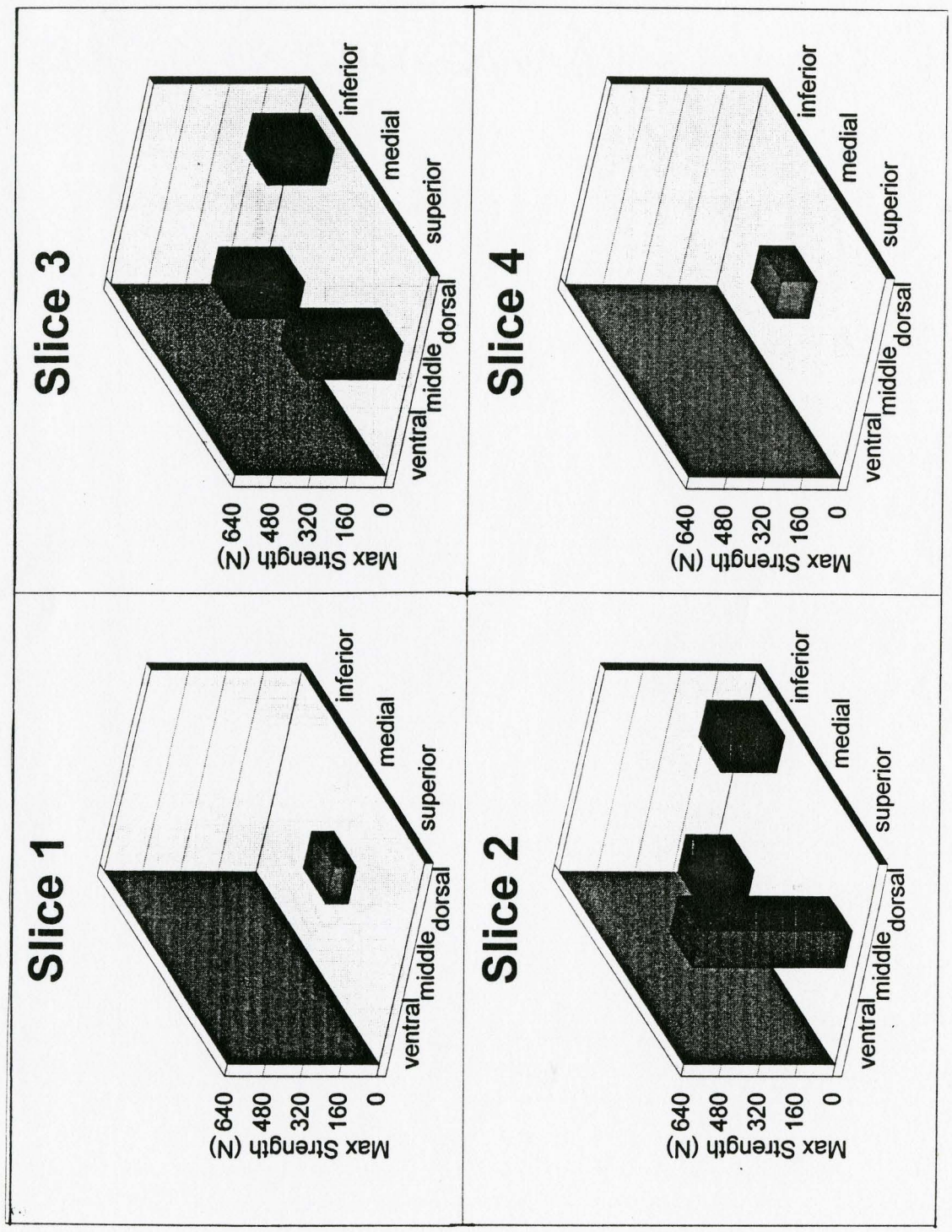

Figure 4.10
Crushing Strength Profile for Femur 4

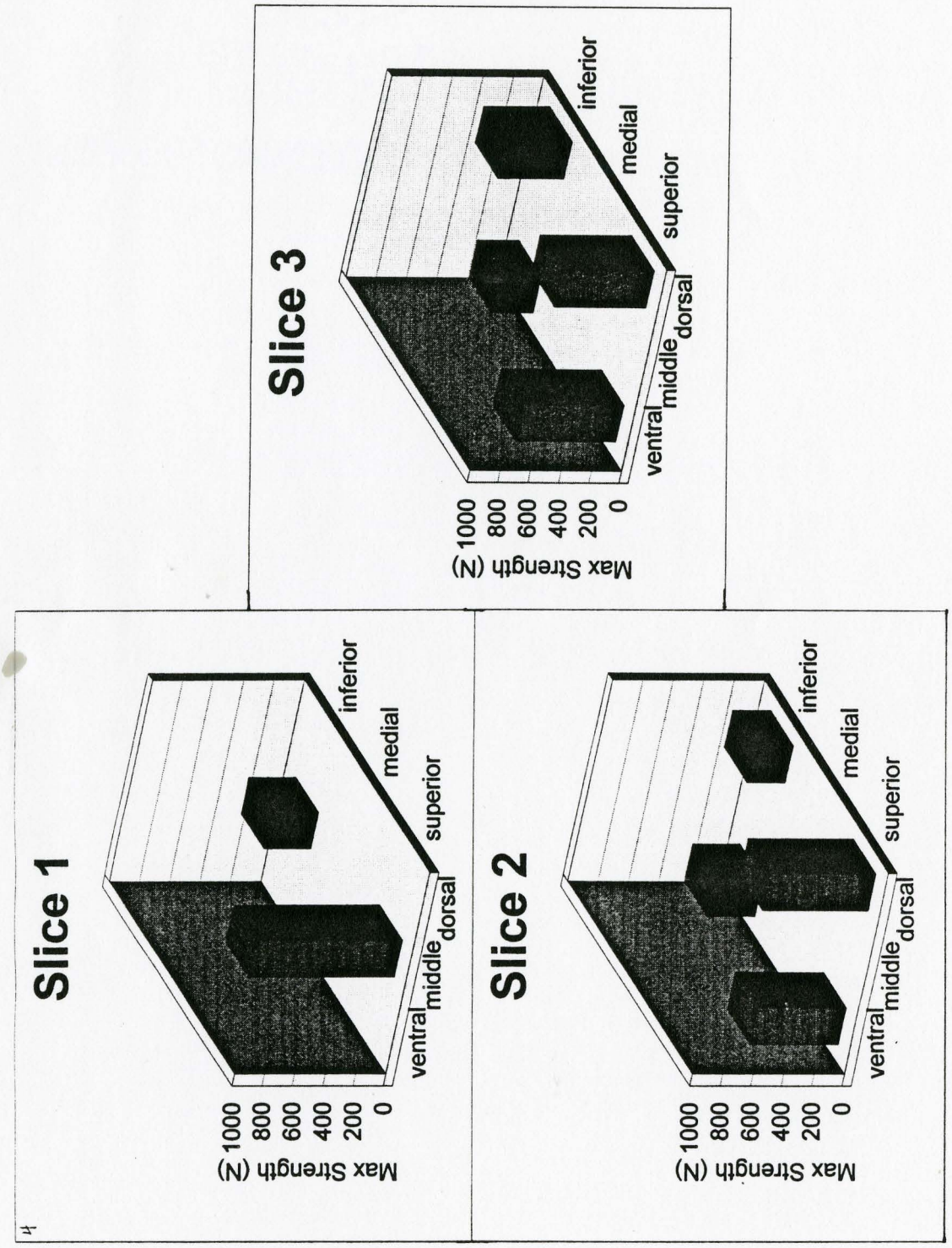

Figure 4.11

Crushing Strength Profile for Femur 5

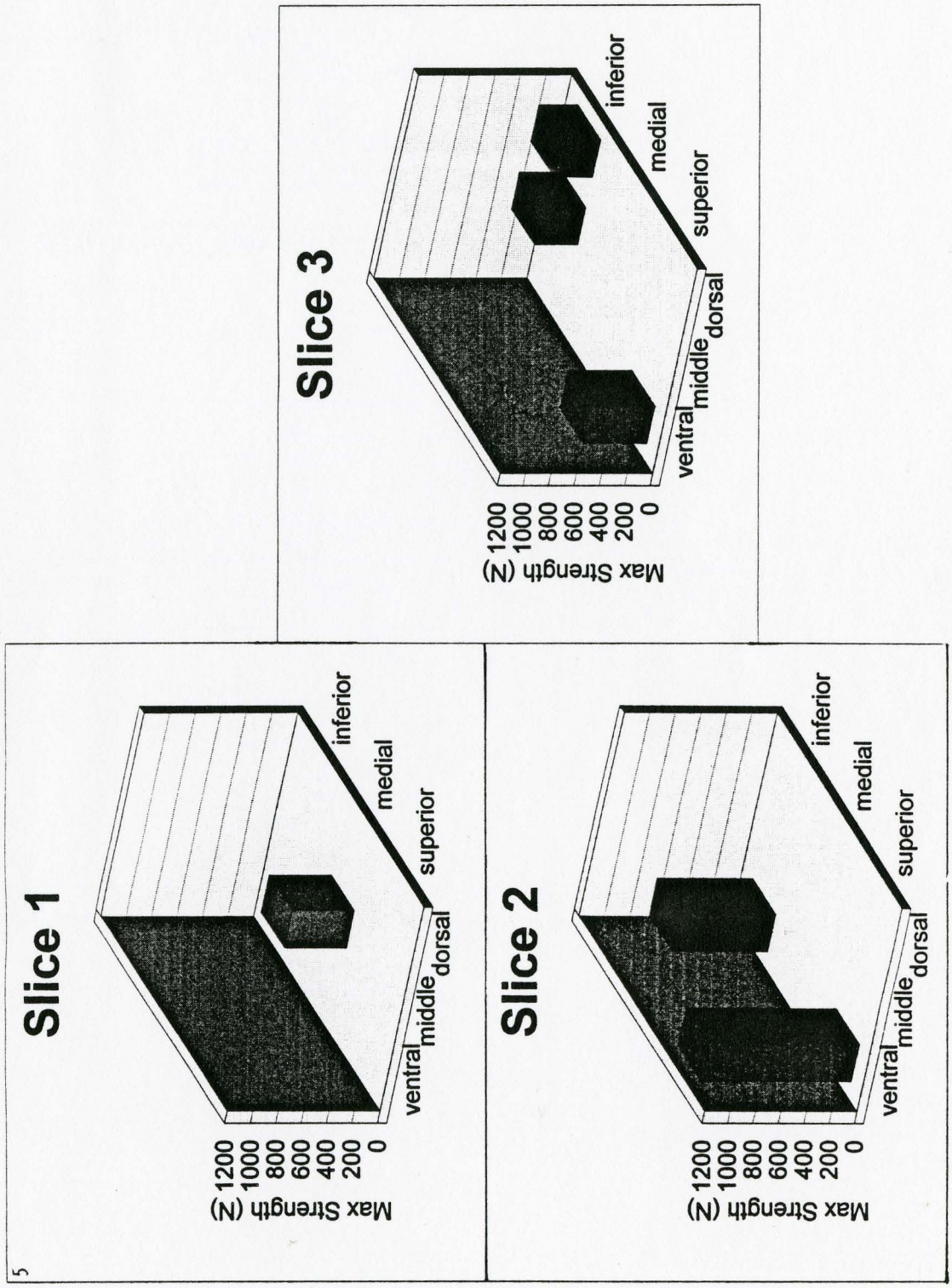

Figure 4.12
Crushing Strength profile for Femur 6

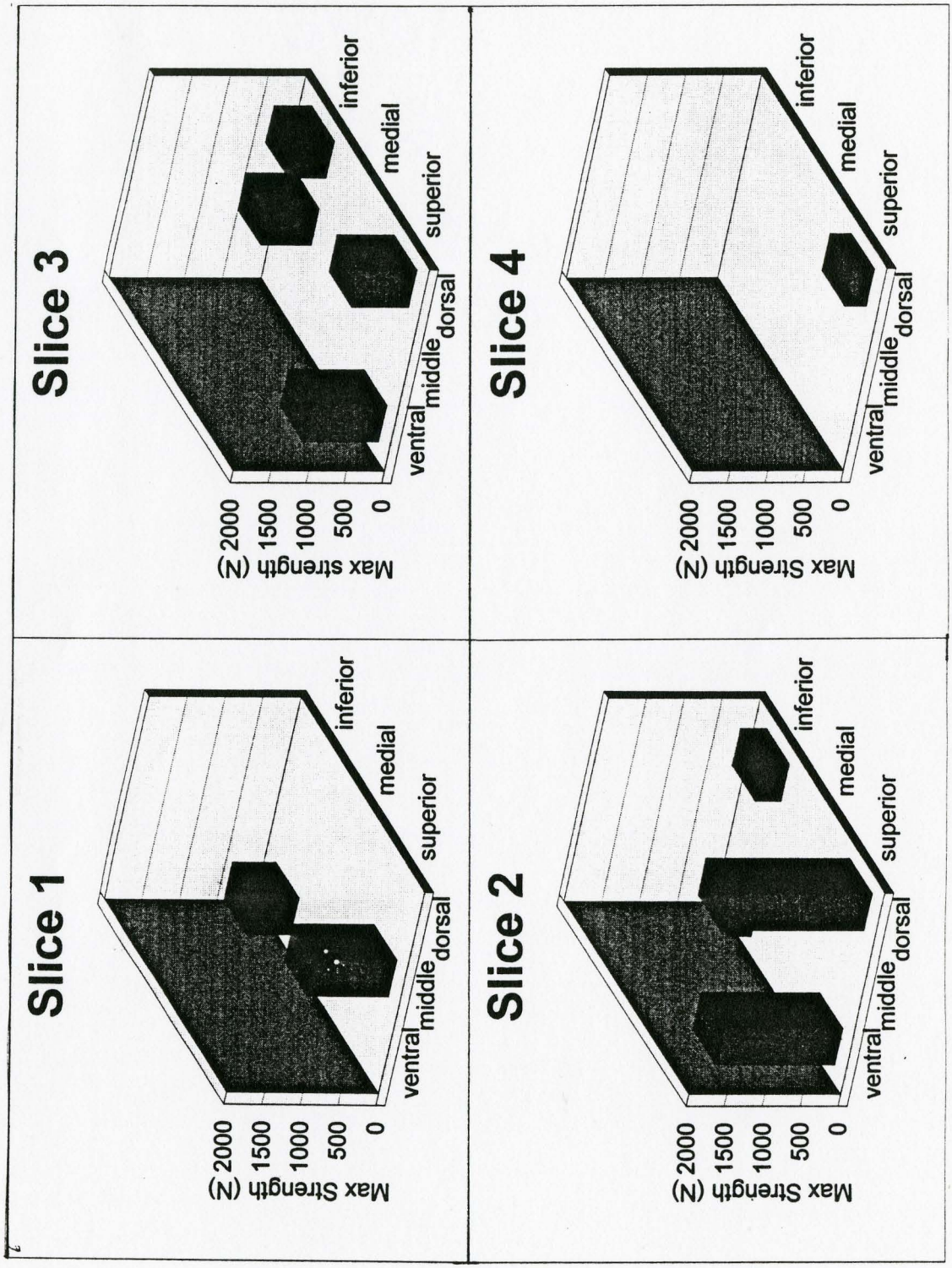

Figure 4.13
Crushing Strength Profile for Femur 7

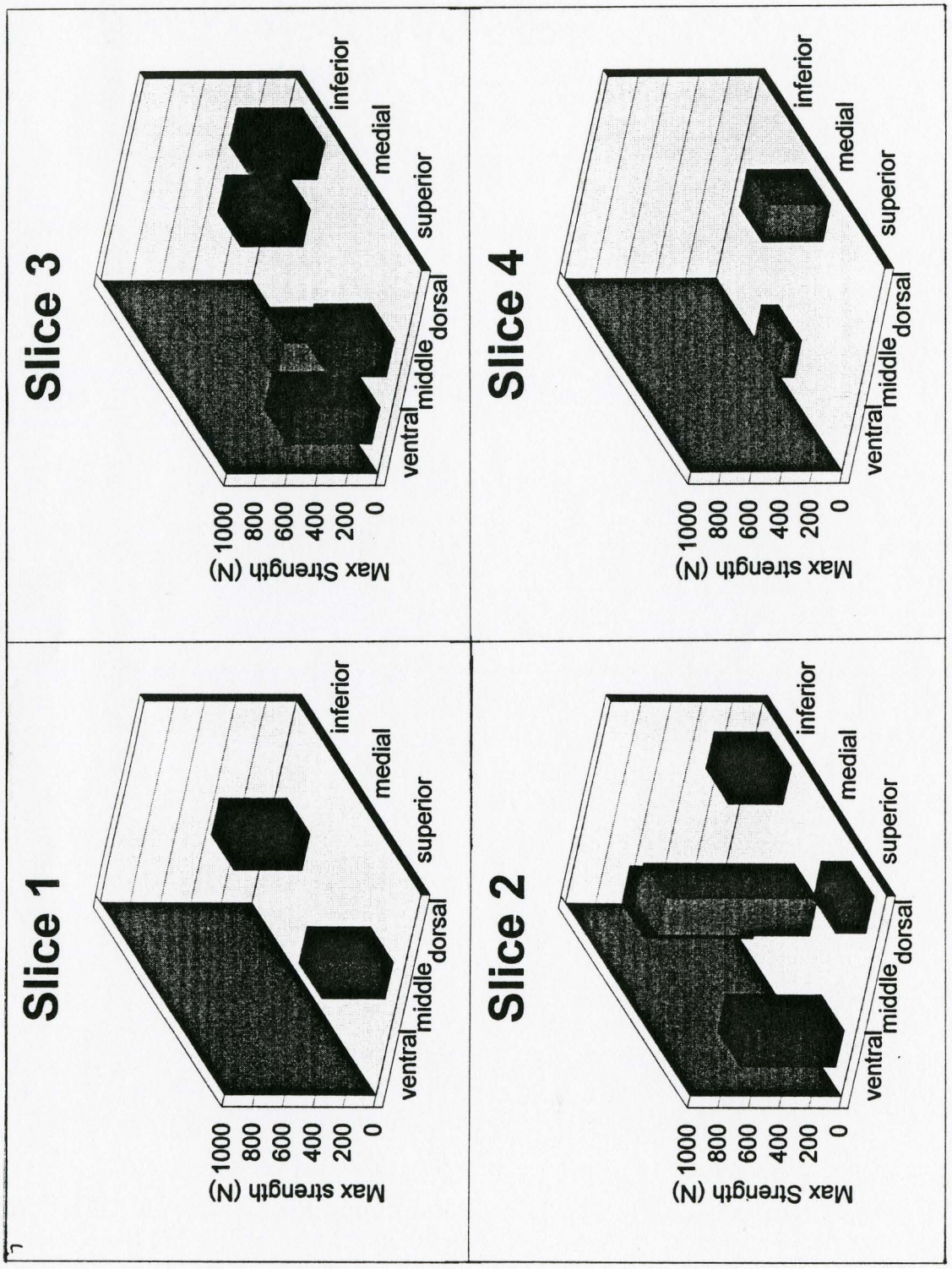

Since this technique is new, a preliminary study was done to see if differences from head to head (inter-sample differences) were larger than differences from slice to slice in the same sample (intra-sample differences). This condition is necessary if the value is to have any actual meaning in distinguishing heads.

Analysis of 2 slices each from 5 femoral head samples (obtained through pathology rather than commercially) were taken. The two slices were taken in a transverse plane close to the centre of the femoral head. The samples were from locations 3.5 mm apart (the slice width). These samples were analyzed as discussed in section 3.7.

The average difference between slices from the same sample (or intra-sample variation) was 8.5×10^{-4} n/p. Standard deviation of average values from sample to sample (or inter-sample variation) was found to be 25.1×10^{-4} nodes/pixel, almost three times larger than the intra-sample difference. The inter-sample variation would certainly be much higher if the same measurements could be done on a more varied study group. Such a group would include samples from young, healthy subjects as well as from elderly, fractured subjects which were all that was available in this case. In a more varied population, the inter-sample variation would certainly be much higher than the intra sample variation.

Chapter 5
Final Experimental Results and Conclusions

5.1 Introduction

After months of collecting, 29 intact femoral head samples were available for this portion of the study. It was not possible to obtain the necessary cores and slices from 5 of these (numbers 4, 6, 9, 24 and 26) since they were too small. Thus these 5 were omitted. This bias should not jeopardize the validity of the study results. We can surmise that these smaller bones would have been weaker and less dense. They would likely have provided points on the lower end of the graphs. We do not expect that they would deviate from the trends we saw. Thus, the omission is only unfortunate in a statistical sense.

Twenty-four samples appear in the results. All these samples come from the pathology departments of either MUMC or Hotel Dieu. They have all been excised, stored in formalin, and baked (see section 3.1) to facilitate cutting. No commercial femurs were used for this portion of the study since they were dry as opposed to formalin-stored. Numerical comparisons of strength or density between the two groups would be invalid due to these differences.

All procedures for obtaining cores and slices are the same as described in chapter 3.

5.2 Results

The data obtained from the 24 samples appears in table 5.1. The matrix of linear correlations for the same data is given in figure 5.2. What are the statistical significances of differences between r values? For example, is the difference between r = .67 for strength vs. ash density statistically different from r = .49 for strength vs. connectivity? The 95% confidence interval for the former is .45 to .89, for the latter .34 to .65. Thus, we cannot confidently say that these two results are meaningfully different. However, looking at the difference between r values for the relationship between connectivity and ash density (r = .34, 95% CI .16 to .52) and work-to-failure vs. ash density (r = .78, 95% CI .70 to .86), we can definitely say that these two values are statistically different.

The relationship between connectivity and strength is shown in figure 5.1. Linear regression gives the equation

$$\text{connectivity} = 1.65*\text{strength} + 0.064 \qquad (5.1)$$

with a coefficient of deviation of 0.24. A log-log plot of the two variables did not improve the fit.

Figure 5.2 shows the relationship between connectivity and ash density. In this case, linear regression gives

$$\text{connectivity} = .008*\text{density} + 0.063 \qquad (5.2)$$

with a coefficient of deviation of 0.11. Again, changing to a log-log scale did not improve the coefficient of deviation.

Figure 5.3 is a log-log plot of maximum compressive strength vs. ash density. Linear regression gives the best-fit line

Table 5.1

Final Test Results

	Sample	Strength	Young's ($\times 10^{8}$)	Work to F	Connect. ($\times 10^{-2}$)	Ash Den.
		Newtons	N/m^2	N-m	Nodes/Pixel	g/cc
1	1	405	1.14	.076	6.66	.207
2	2	1950	7.13	.353	6.76	.471
3	3	670	2.86	.095	5.99	.205
4	5	710	2.91	.137	6.63	.269
5	7	1130	3.72	.248	6.28	.419
6	8	2350	8.84	.482	7.07	.424
7	10	650	2.44	.140	6.56	.371
8	11	240	.80	.120	6.70	.194
9	12	315	5.18	.279	6.65	.449
10	13	657	2.21	.163	6.22	.248
11	14	1440	5.85	.300	6.69	.293
12	15	805	3.52	.121	6.56	.225
13	16	1180	4.93	.218	6.47	.323
14	17	350	1.10	.081	6.59	.211
15	18	1320	4.09	.380	6.76	.245
16	19	2970	10.71	.520	6.80	.431
17	20	385	.97	.092	6.17	.183
18	21	1060	2.10	.335	6.37	.425
19	22	444	1.20	.103	6.23	.218
20	23	135	.57	.028	6.39	.200
21	25	530	1.42	.122	6.68	.205
22	27	140	.79	.025	6.56	.115
23	28	425	1.18	.088	6.51	.262
24	29	1110	5.31	.154	6.56	.296

Strength = Maximum Compressive Strength
Young's = Young's Modulus of Elasticity
Work to F = Work to Failure
Connect. = Connectivity
Ash Den. = Ash Density

Table 5.2

Correlation Matrix for
Final Test Results

Linear Regression

Correlation Matrix for Variables: X_1 ... X_5

	Connect.	Strength	Ash Den.	Young's	Work to F
Connect.	1				
Strength	.492	1			
Ash Den.	.337	.674	1		
Young's	.536	.928	.726	1	
Work to F	.534	.899	.782	.871	1

Figure 5.1

Connectivity vs. Strength

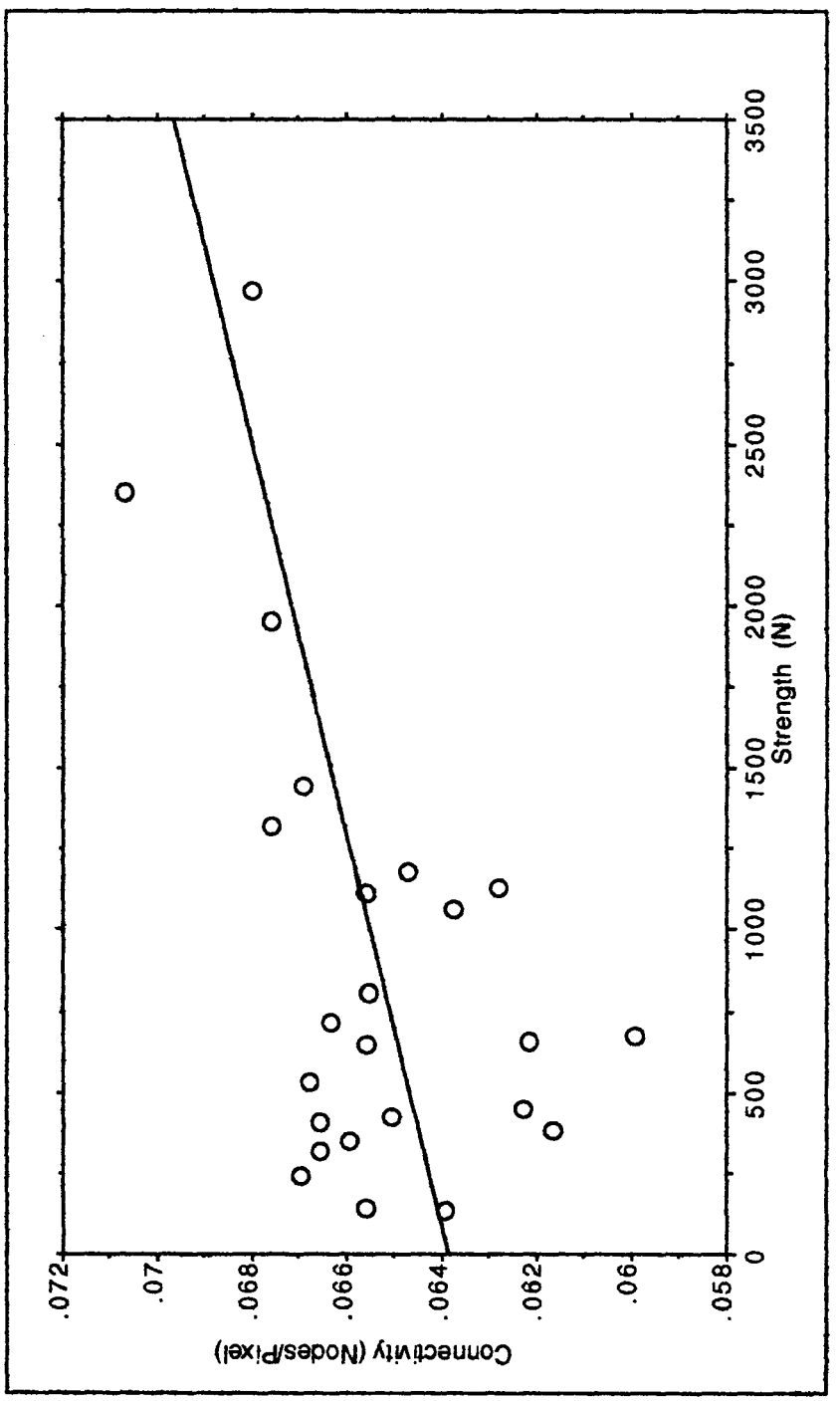

Figure 5.2

Connectivity vs. Ash Density

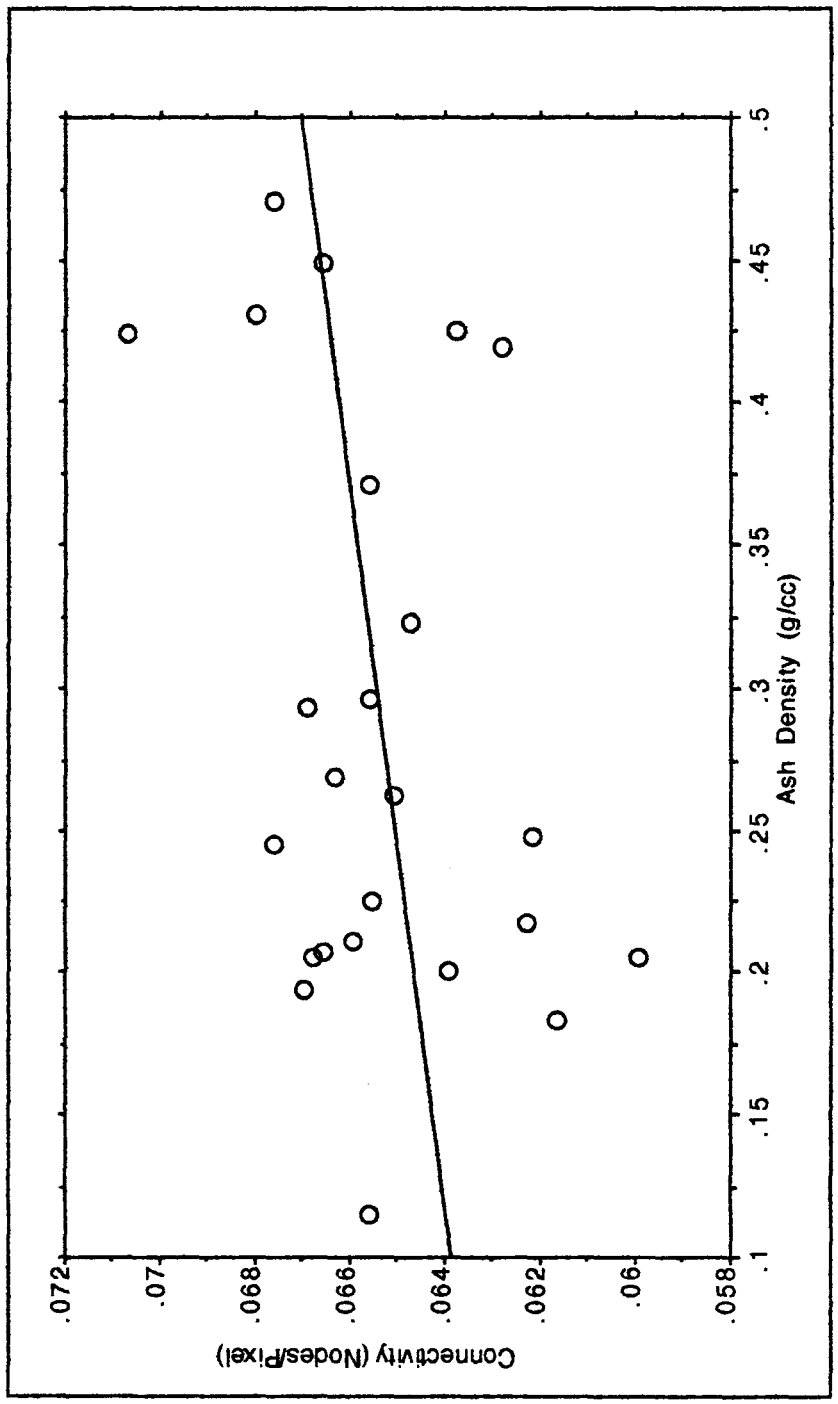

Figure 5.3

ln-ln Plot of Strength vs. Ash Density

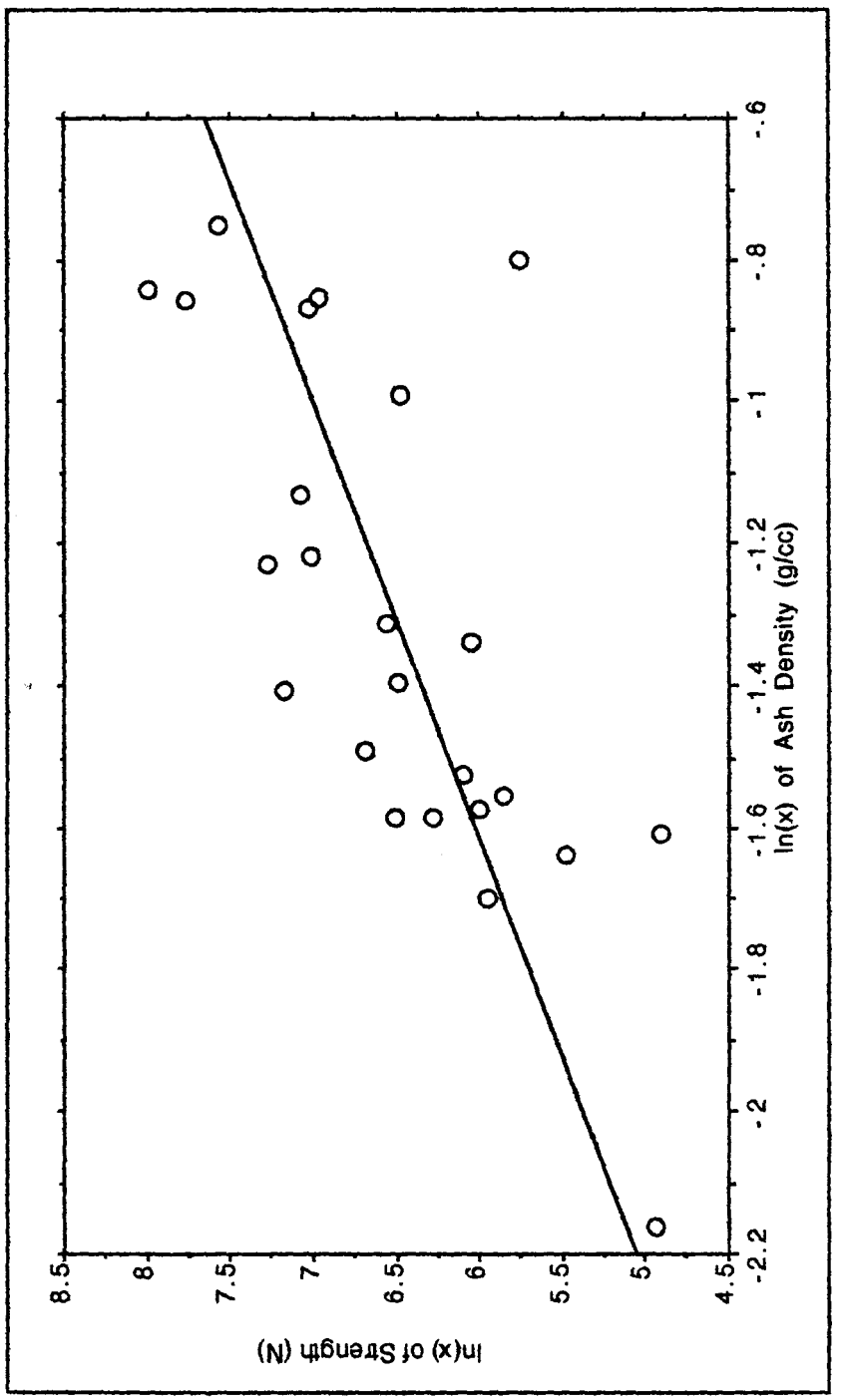

$$\text{strength} = 1.62*\text{density} + 8.614 \qquad (5.3)$$

This logarithmic plot gives a better fit ($r^2 = .52$) than a linear plot of the same variables ($r^2 = .46$). This suggests that the relationship between maximum compressive strength and ash density suits a power law proportionality with an exponent of n=1.62, ie:

$$\text{strength} \; \alpha \; \text{density}^n \qquad (5.4)$$

Figures 5.4 and 5.5 are log-log plots of Young's modulus vs. ash density and work to failure vs. ash density respectively. Similarly, log-log plots give better fits than their respective linear plots. r^2 values improved from 0.53 to 0.59 and from 0.61 to 0.69 for figures 5.4 and 5.5 respectively. Linear regression of figure 5.4 gives

$$\text{Young's modulus} = 1.78*\text{density} + 21.652 \qquad (5.5)$$

and figure 5.5 gives

$$\text{work to failure} = 1.82*\text{density} + .475 \qquad (5.6)$$

which correspond to n = 1.78 and n = 1.82 in equation 5.4.

Residual analysis of the data was done, where residuals from the log-log plot of work-to-failure vs. ash density were plotted against connectivity. This graph is shown in figure 5.6. Regression analysis gave an r^2 of 0.074 for the equation

$$\text{residual} = 49.9*\text{connectivity} + 3.26 \qquad (5.7)$$

Figure 5.7 is the result of an attempt to see if connectivity

Figure 5.4

Log-log Plot of Young's Modulus
vs.
Ash Density

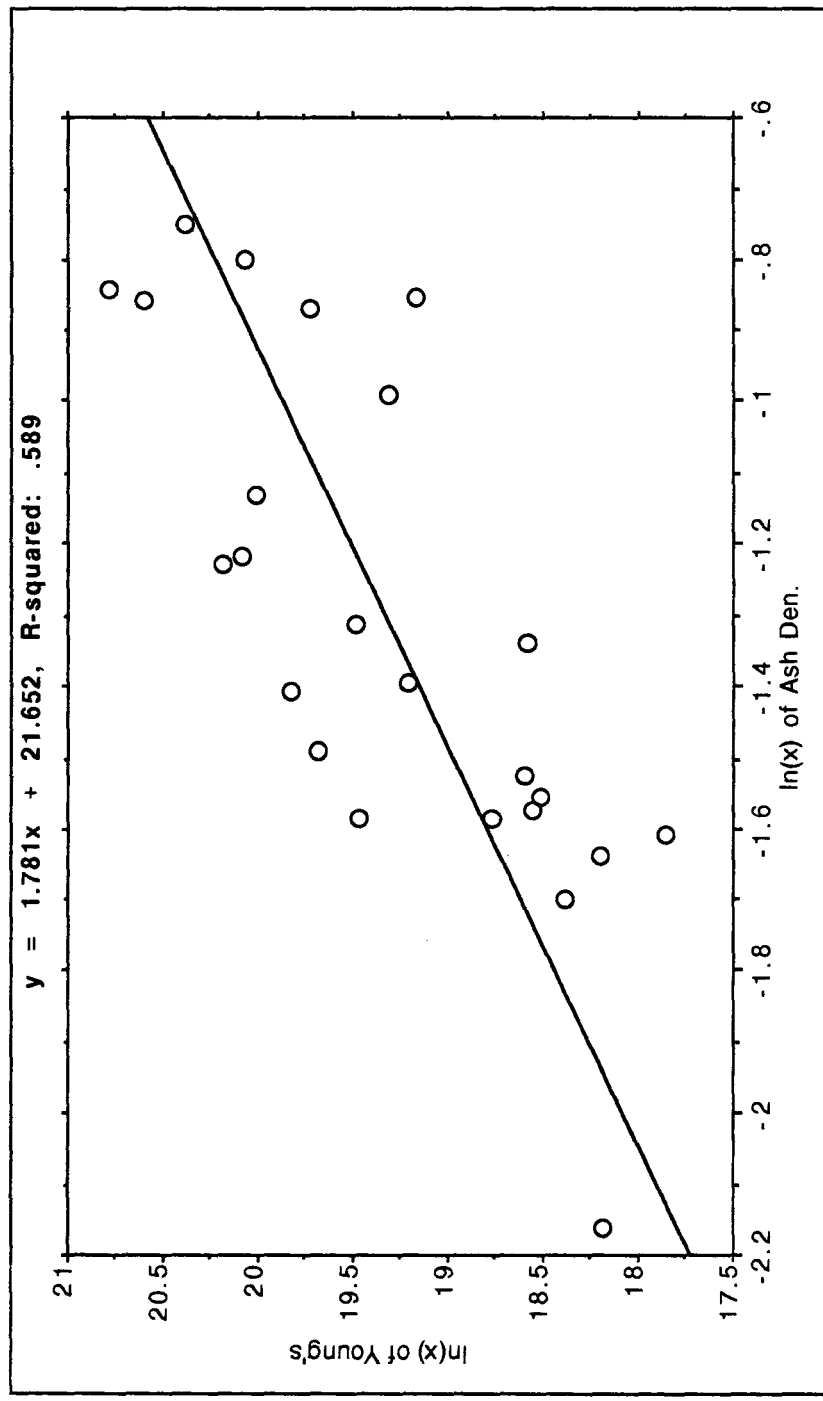

Figure 5.5

Log-log Plot of Work-to-Failure
vs.
Ash Density

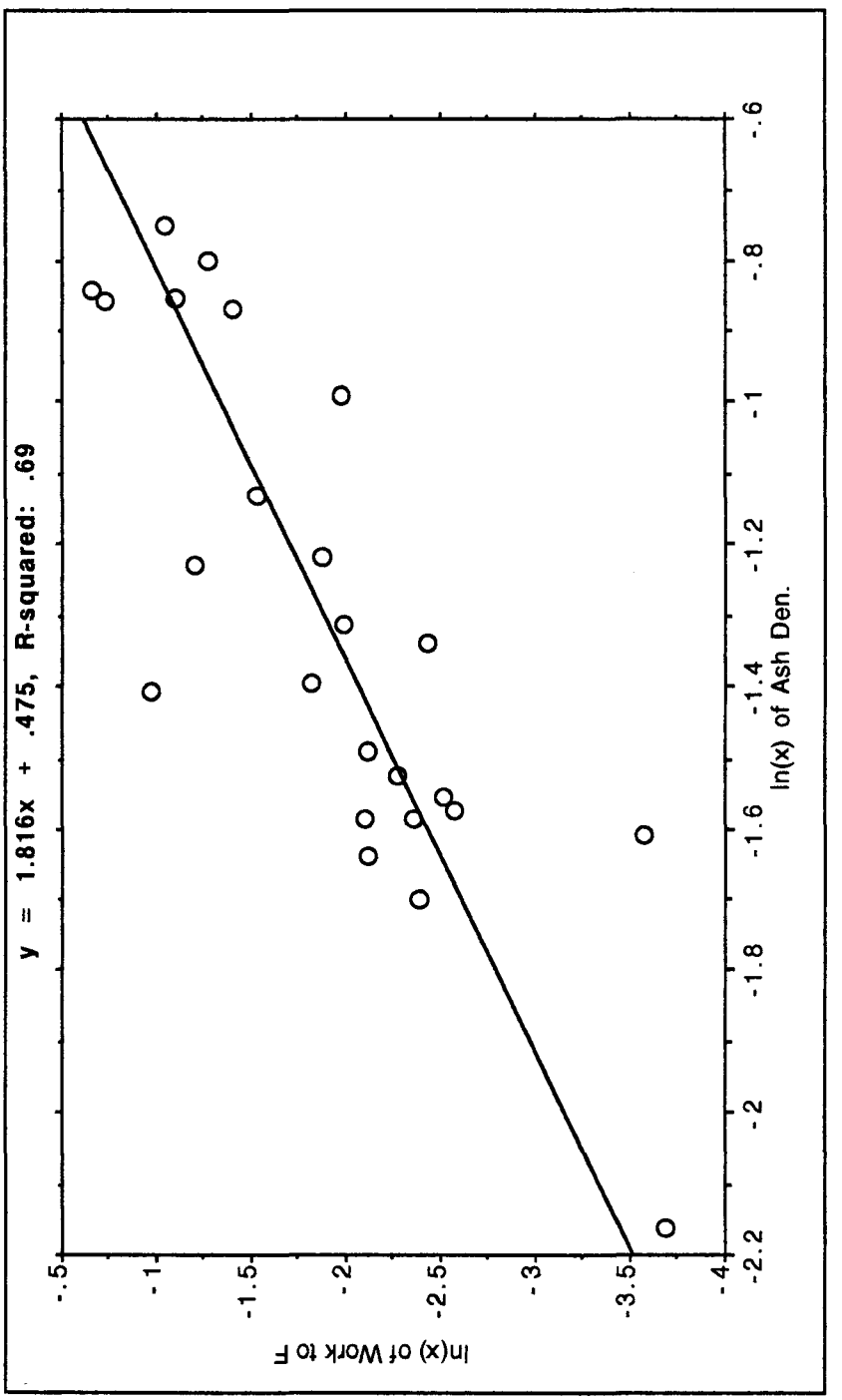

Figure 5.6

Residual of ln(Work-to-Failure) vs. ln(Ash Density)

: versus

Connectivity

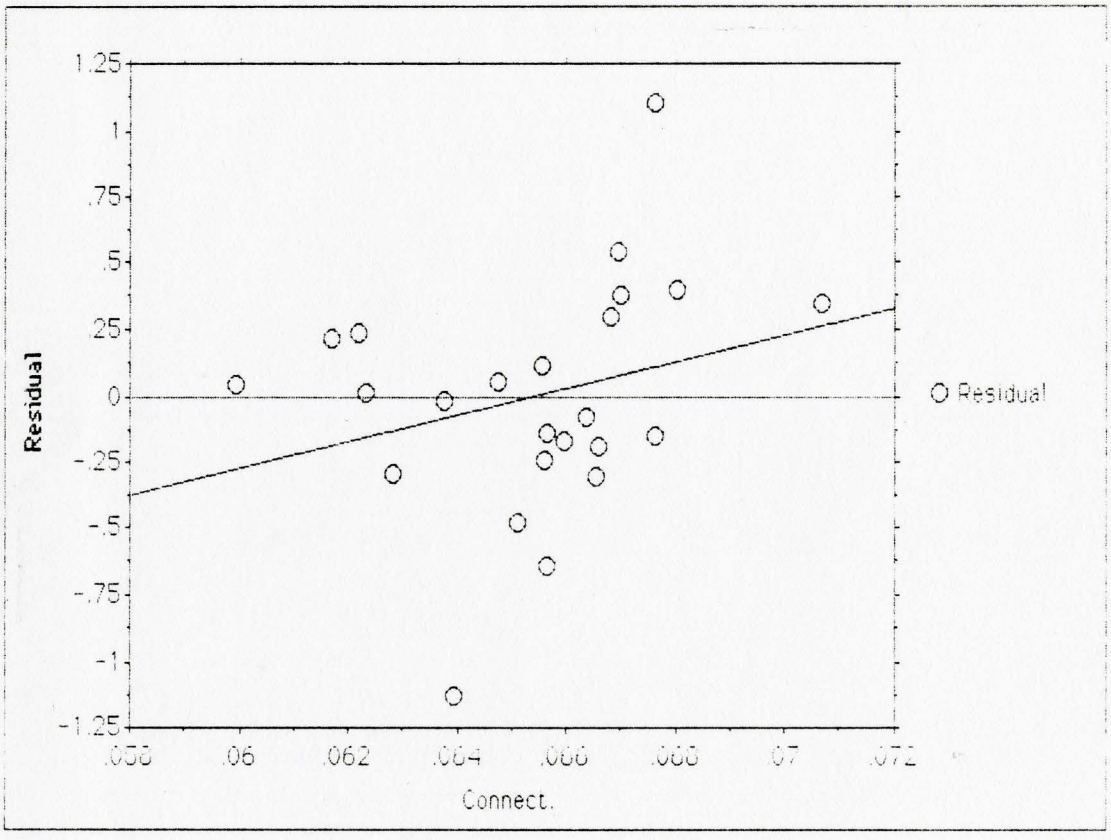

Figure 5.7

ln(work-to-failure)
versus
combined connectivity and ash density

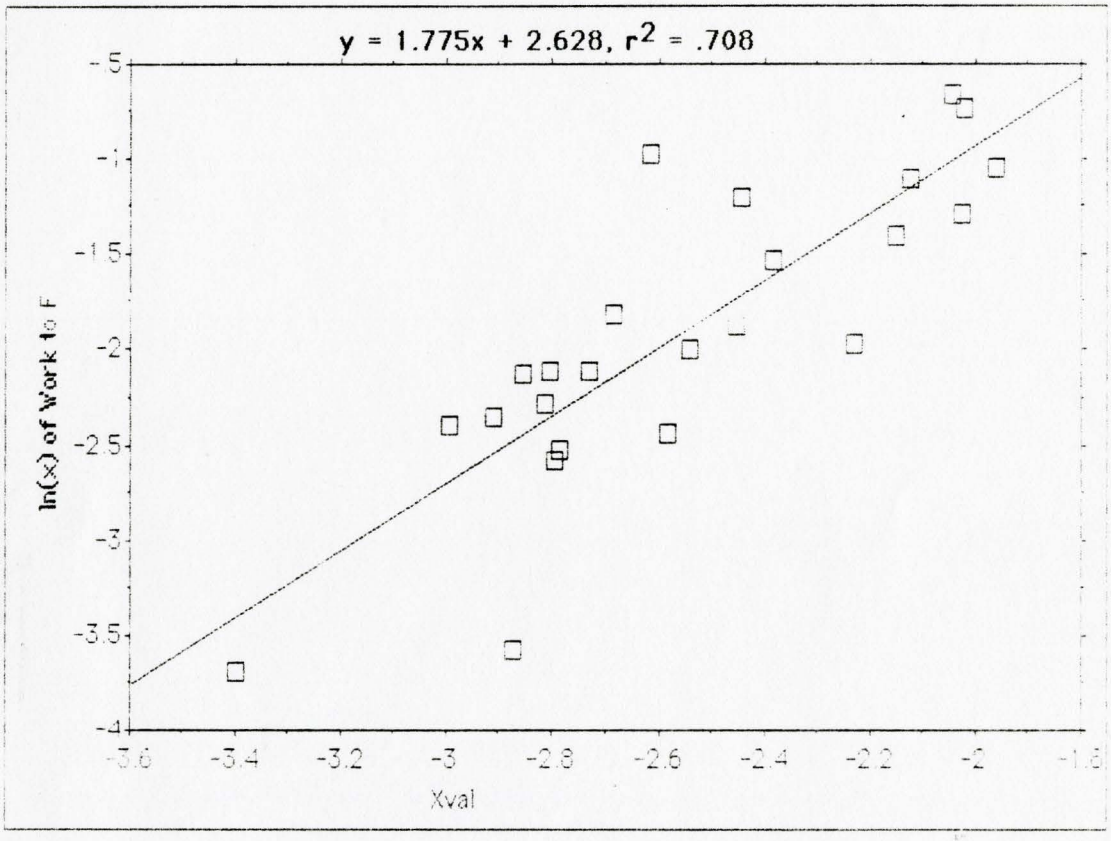

values could be used to improve prediction of bone strength from ash density, the following procedure was followed:

1) ash density and connectivity were scaled to the same mean value,
2) the logs of these two scaled variables as well as work-to-failure were taken,
3) The logs of scaled connectivity and ash density were added and the result called Xval, and
4) The log of work-to-failure was plotted vs. Xval.

Linear regression of figure 5.7 gave

$$\ln(\text{work-to-failure}) = 1.78*\text{Xval} + 2.63 \qquad (5.8)$$

with an r^2 of 0.71.

5.3 Discussion

Optimum correlations for the mechanical parameters were obtained with linear plots when connectivity was the independent variable and with logarithmic plots when ash density was the independent variable.

It was noted that there was only a small variation in the connectivity values, which ranged from .060 to .071 nodes/pixel with a standard deviation of 0.002 and a coefficient of variation of 3.7 %. Compare this with coefficients of variation of 35.6 % for ash density and 80.1 % for maximum compressive strength. Subjects from whom these samples were obtained ranged in age from 42-84 years. The age standard deviation was 9.1 years and the coefficient of variation 13.12 %. The study group was further specified by the fact that all individuals had fractures of the proximal femur serious

enough to warrant replacement surgery. It would be interesting to know if samples from a more varied population (ie: younger, healthier, unfractured subjects as well) would show a greater range of connectivity values. Could it be that all connectivity values seen are very low if compared to the value for a young, healthy subject? In this case connectivity could indeed be a good indicator of fracture risk.

The result shown in equation 5.4 agrees reasonably well with the findings of Carter and Hayes [25] who found a coefficient of 2.0 rather than 1.6 when plotting maximum compressive strength against ash density. Their testing method was slightly different, in that the bone core was contained in a rigid cylinder during crushing. The work-to-failure and Young's modulus data gave coefficients closer to 2.0 when plotted against ash density.

What are these results saying about relationships between connectivity, ash density and bone strength as quantified in the three different ways?

Table 5.2 gives the linear correlation matrix for the strength and structure variables. Note that the correlations between maximum compressive strength, Young's modulus, and work-to-failure were extremely high ($r = 0.87$, 0.90, and 0.93). This is expected since all three are measures of the physical resistance of the same bone core. The weakest correlation was between ash density and connectivity. This is an important result since it implies that connectivity (architecture) is not totally dependent on bone density. The fact that architecture can vary independently of bone mass leaves open the possibility that it is an independent determinant of bone strength.

Ash density and connectivity were generally best correlated with work-to-failure ($r^2 = 0.69$ and 0.29 respectively). Young's modulus

correlated almost as well (r^2 = 0.59 and 0.29). Of the parameters obtained from the crushing curve, maximum compressive strength gave the weakest correlation with connectivity (r^2 = 0.24) and ash density (r^2 = 0.52). Since we do not know which of the crushing curve variables is the most significant in predicting resistance of a bone to fracture, we must consider all three, not weighting one more than another.

The final goal of the thesis was to address the question of whether connectivity is an important factor in determining bone strength. Correlations between connectivity and the three bone strength variables were weaker than correlations between ash density and these variables. Thus, if we had to choose just one variable to quantitate bone strength, ash density is a better choice than connectivity. But as is shown by figure 5.7, a slight improvement (r^2 increases from 0.69 to 0.71) in predicting bone strength (as measured by work-to-failure) can be made by introducing an architectural factor.

Although the correlation of connectivity to the three crushing curve variables was quite weak (r^2 = 0.24 to 0.29), they were better than those between connectivity and ash density (r^2 = 0.11). This implies that connectivity is relatively independent of bone density and may have some independent predictive value in determining bone strength factors.

Chapter 6
pQCT: Towards an In-Vivo Architecture Measurement

All work in this chapter was done on a newly-installed Stratec pQCT scanner system at Dr. J.D. Adachi's office at

Hamilton Osteoporosis Clinic
25 Charleton Ave. E.
Suite 501
Hamilton, Ont.

6.1 An Introduction to pQCT

pQCT (Peripheral Quantitative Computed Tomography) is a recently developed in-vivo method of measuring a bone mass. The only currently available commercial machine is produced by Stratec[10]. Figure 6.1a shows the machine. The patient is seated comfortably with her arm inserted into the source/detector ring. The length of the forearm has already been measured between the

[10] Stratec
Medizintechnik
Gewerbestrabe 11
D-7534 Birkenfeld 2
West Germany

In North America
Norland Corporation
Norland Drive
Fort Atkinson, Wi 53538
U.S.A.

Figure 6.1 a and 1b

1a The pQCT System

1b The Rotate/Translate Mechanism

1a

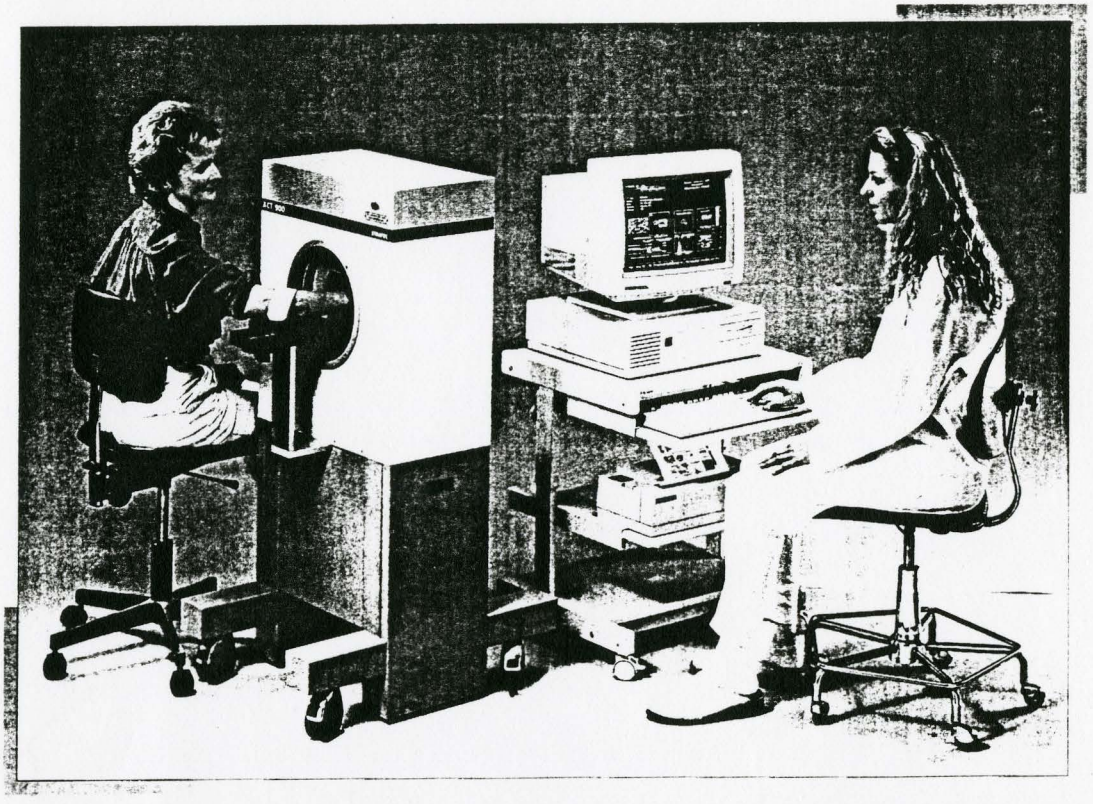

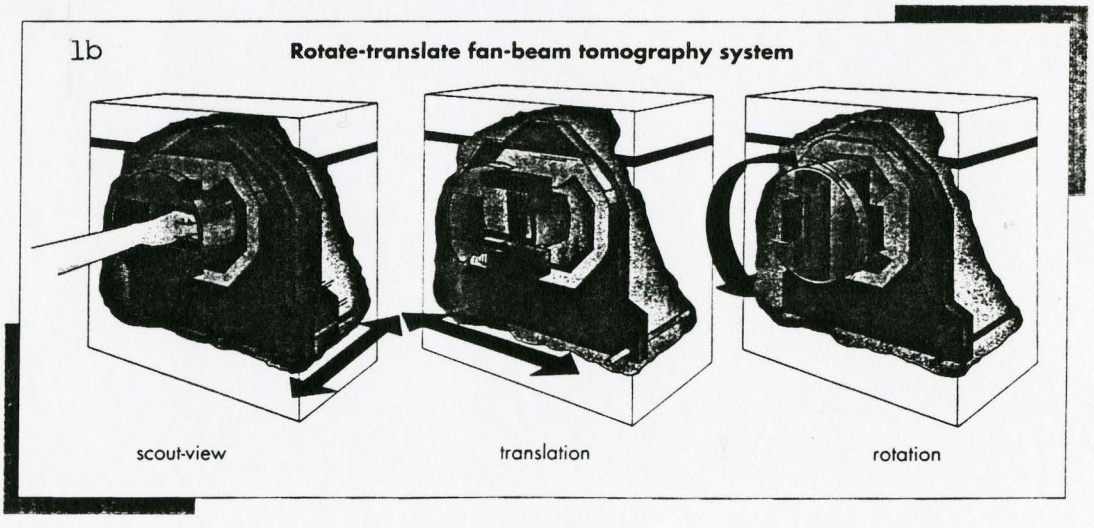

proximal tip of the radius and the lateral epicondyle at the distal end of the ulna. This measurement is used to set the arm restraining mechanism to a patient-specific length.

Figure 6.1b shows the rotate/translate mechanism which allows the pQCT scanner to take both conventional x-rays (translate) and CT images (rotate). The machine first takes a standard 2-D projected x-ray of the distal region of the forearm. This is known as the "scoutscan". The initial arm positioning procedure ensures that the scoutview will contain the region of interest; that is, the end plate of the radius and the region proximal to this. From this image the position of the plate at the distal end of the radius is marked by the operator. The computer then measures proximally along the radius a distance which is 4 % of the length of the previously measured length of the subject's forearm. It is here that the CT slice, which provides the quantitative information, is taken. The CT slice is taken using the system's rotate capability. 15 different transmission views of the arm are taken around 360^0 (24^0 between each scan). The computer pieces together these 15 views into a filtered back projection image showing a "transverse slice" of the radius, ulna, and soft tissues. A typical image is shown in figure 6.2. Landmarking using the end of the radius is an important feature of this system since the ability to relocate the slice in the same anatomical position will be the primary determinant of reproducibility. Some of the manufacturer's specifications for the system are given in table 6.1.

The "peripheral" in pQCT refers to the bones being scanned, which are part of the peripheral, as opposed to the axial, skeleton. The forearm has a high bone-to-soft tissue ratio (as opposed to the abdomen or hip), and is relatively radioinsensitive. Thus good resolution can be obtained at a low dose equivalent to the patient

Figure 6.2

A Typical pQCT Measurement

STRATEC XCT-960 PQCT^{cm}

HAMILTON OSTEOPOROSIS CLINIC 25 CHARLTON AVE. E. SUITE 501
HAMILTON, ONTARIO

NAME: Average, Jane Q.
CT.NO.: 00107L GENDER: female LENGTH OF FOREARM: 264 mm
DOB.: 10-12-24 DATE OF SCAN: 04-15-93 AGE: 68

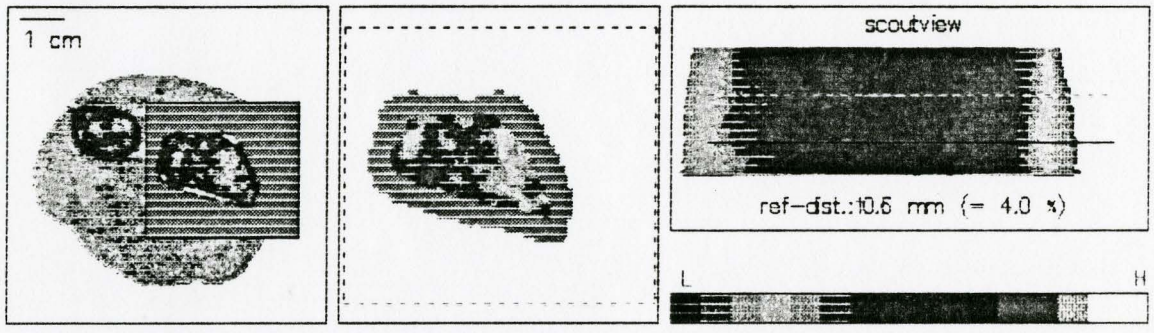

Referenz:

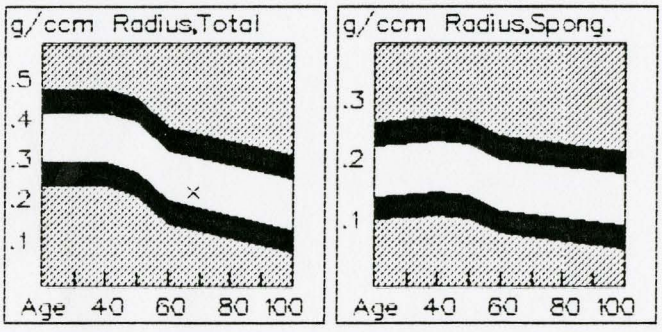

	Total	Trab.bone	Cort.(sub)
Density:	227.9	107.1	326.6
[mg/ccm]	±5.0	±3.0	±9.0
Tscore:	-2.3	-2.2	
Zscore:	-0.5	-1.3	
#Voxels:	930 (323.7 mm²)		

THRESHOLD - 0.50 Trab.area - 45.0% Voxel size - 0.590mm Referenz -GER02 CALCBD V 5.0

COMMENTS:

Table 6.1
Manufacturer's Specifications for The pQCT System

The scanning site is determined precisely before the CT-scan is started by means of a scout scan of the distal forearm. After positioning the CT-cross-sectional plane, the rotate-translate procedure is started to generate the absorption-profiles for the computed tomogram.

A special ultra-stable x-ray tube is used to generate an x-ray fan beam.

The detectors are equipped with a newly-developed array of semiconductors. The use of an arry significantly shortens the scanning time.

Internal operation of three axes of movement as well as simultaneous data processing is controlled by means of microcontrollers.

Performance Specifications

Scan Site	Forearm - distal radius
in vivo Precision	Trabecular: ± 3 mg/cm^3; Total: ± 5 mg/cm^3: Cortical ± 9 mg/cm^3
Accuracy	Within 2%
Dose	CT Scan - 3 mR (.03 mSv) typical Scout Scan - 3 mR (.03 mSv) typical
Leakage Radiation	< 1 mR/hour (.01 mSv/hour), only during scans
Spatial Resolution	B = .59 mm (Voxel size); A = .689 mm
Scan Time	2.5 minutes - Scout Scan 2.5 minutes - CT Scan
Procedure Time	Typically less than 15 minutes
Conditions of Operation	45 kV X-Ray Tube Voltage; <.3 mA X-Ray Tube Current; 2.5 mm Section thickness; >5 mm Al Filtration; 5 minutes exposure (Scout scan plus CT scan)

continued...

Technical Details

1. Detector Unit - 6 semiconductor detectors with amplifiers

2. x-ray tube (XCT)

High Voltage	45 kV
Anode Current	< .3 mA
Mean x-ray energy	38 keV
Width of energy beam (after filtering)	8 keV (FWHM)

3. Scanner Mechanics
   - Linear scan path: 120 mm
   - Translation-Rotation fan beam principle
   - Scan time: 8s
   - Range of Angulation: 180°
   - Rotation around Centre: 200°
   - Position shift speed: 6°/s
   - Axial movement (> scout view <)
   - Maximal length of path: 50 mm
   - Speed: 3 mm/s
   - Interface for positioning: V.24, 9600 Bd.
   - Central Gantry opening: 120 X 200 mm
   - Weight: approx. 90 kg.
   - Power Supply: 220/110 V, 50-60 Hz, 80 VA
   - Base 560 X740 mm mobile unit with 2 brakes
   - height 1250 mm

4. Computer System
   - 32 bit computer (with 80386 or 80486 processor and math coprocessor)
   - 1 MB RAM memory minimum
   - VGA color graphic card and 14" color monitor
   - 110 MB hard disk
   - 1.4 MB floppy drive 3.5"
   - two V.24 interfaces for control unit/scan data transfer and connection to central computer
   - color printer or laser printer

(.06 mSv or 6 mR for both scout scan and CT scan as stated by the manufacturer). The volume of tissue irradiated for the measurement scan is a slice of thickness 0.7 mm. Compare this to a DPA hip scan which gives a similar dose equivalent to a larger volume of tissue and provides less information.

It is the radius, as opposed to the ulna that is used for quantifying the bone density. The effect of physical activity upon bone density is considered to be minimized by using the non-dominant arm.

From the linear attenuation coefficients measured by the machine, bone density is calculated at each pixel and a color picture (a "density map") produced. Density is expressed in mg/cm^3. The transverse slice view of the radius allows the cortical shell and inner trabecular mesh to be separated and analyzed independently. A weighted mean bone density for each is calculated, as well as an overall weighted mean (see figure 6.2). Trabecular bone densities seen in this study ranged from 50-325 mg/cm^3. Cortical densities ranged from 250-781 mg/cm^3. Total (weighted mean) values ranged from 140-550 mg/cm^3. Thus more information can be obtained than from a standard two-dimensional projection method such as DPX, where the measured bone mass represents the amount of mineral at the measurement site irrespective of whether it is trabecular or cortical.

It is hoped that the image provided by the pQCT scanner can be used to quantitatively analyze the trabecular network in the same way as the high-resolution in-vitro bone slice x-rays.

6.2 Testing the pQCT System

This being a new system, it was considered important to address

four questions:

1) How reproducible are the measurements with the system used in this study? (The manufacturer states greater than 1% reproducibility in-vivo)

2) Is handedness significant to the measurements?

3) Do measurements in the forearm (pQCT) correlate with measurements in the hip or spine (DPX)

4) Might additional information be available from the distinction of trabecular from cortical bone?

To answer question 1, eight subjects were scanned more than once. The subject's arm was repositioned for each measurement. The results are given in table 6.2. There is one apparently anomalous result. The scans of subject 6 cannot be validly compared as inaccurate landmarking has meant that the two measurements are at slightly different locations. It is interesting that while cortical values are very different between the 2 scans, total and trabecular values agree. How is this possible in light of the fact that total values are averages of cortical and trabecular? The answer is that different areas of bone have been scanned in each case. Thus weighting factors for cortical and trabecular components used in calculating the total result would not be the same.

Besides this result, mean coefficients of variation were between 1.5 and 1.8%. The data suggests that reproducibility improved as the operator became more experienced. These mean values may therefore be slight overestimates for a rigorous, experienced operator. Most of the variation probably arises from slight differences in the position of the image slice from trial to trial. This error could be reduced by having the same operator perform all measurements, as there is a small amount of subjectivity in selecting the landmark (end plate) from the scoutscan image. Error

Table 6.2

Results of Reproducibility Testing

Reproducibility has been expressed as the coefficient of variation (CV)

	Subject	Total	Trab	Cort	CV Tot	CV Trab	CV Cort
		mg/cc	mg/cc	mg/cc			
1	1	391.0	195.5	564.4	4.8	1.0	5.2
2	1	429.9	192.1	625.7	•	•	•
3	1	417.9	195.2	605.5	•	•	•
4	2	475.3	193.1	693.6	1.5	3.5	.2
5	2	465.2	183.7	695.2	•	•	•
6	3	481.6	160.2	750.8	1.8	.4	1.5
7	3	469.4	161.2	735.0	•	•	•
8	4	542.8	320.3	584.8	1.2	1.3	.8
9	4	552.4	326.4	591.2	•	•	•
10	5	441.2	258.8	528.5	2.2	2.5	1.6
11	5	427.7	249.7	516.8	•	•	•
12	6	528.1	280.6	781.1	.9	.8	18.2
13	6	521.5	277.4	603.3	•	•	•
14	7	441.4	244.5	551.0	1.4	2.3	.7
15	7	429.3	234.3	546.7	•	•	•
16	7	435.0	242.7	542.9	•	•	•
17	8	448.2	249.7	610.2	.6	.4	.9
18	8	444.4	251.0	602.5	•	•	•
19	mean	•	•	•	1.8	1.5	3.6
20	mean*	•	•	•	•	•	1.6

* excluding subject 6

stemming from the measurement system itself could be assessed by repeating measurements without repositioning between scans.

To illustrate the importance of good reproducibility the pQCT system was used to search for an effect of handedness on bone density in the distal radius. Six subjects had their left and right radii measured. All subjects were right-handed. This information appears in table 6.3. Subject 1 produced notable results. He had previously broken his right (dominant) wrist. The "weld" produced when the bone healed greatly increased bone density. This is reflected in his right trabecular bone density being 72% higher than in the left radius. For the other 5 subjects, left-right differences were generally greater than the reproducibility. For trabecular bone, all 5 subjects showed differences more than 3 times the CV. For cortical bone, only 2 subjects showed dramatic differences. However, it should be noted that the differences did not always correspond to handedness and it must be postulated that factors other than laterality must affect bone density in the distal radius.

To address question 3, 49 subjects who were attending a metabolic bone disease clinic and who had recently had DPX measurements of the hip and spine were scanned on the pQCT scanner. The DPX measurements were done on six different Lunar DPX machines at St. Joseph's Hospital. The results are listed in table 6.4. If pQCT and DPX systems were equally adept at evaluating a person's bone mass (thereby fracture risk), a straight line should be obtained when the DPX result is plotted against the pQCT result. The results for the comparison of total radius bone mass with the femoral neck and lumbar spine bone mineral densities are shown in figures 6.3 and 6.4. These figures display considerable scatter. Table 6.5 shows the correlation matrix for the measured variables. These results show that the radius trabecular bone mass displays

Table 6.3

Comparison of Bone Mass in Both Arms
in Six Right-Handed Subjects

	Subject	Arm	Total	Trab	Cort	Tot diff	Trab diff	Cort diff
			mg/cc	mg/cc	mg/cc	%	%	%
1	1	L	470.3	188.4	694.4	•	•	•
2	1	R	589.8	400.3	703.9	2.10	72.00	1.40
3	2	L	364.0	162.6	528.5	•	•	•
4	2	R	424.0	171.8	629.5	15.20	5.50	17.40
5	3	L	434.5	254.3	522.7	•	•	•
6	3	R	470.1	279.6	551.6	7.90	9.50	5.40
7	4	L	338.3	182.2	465.9	•	•	•
8	4	R	326.4	166.6	457.2	-3.60	-8.90	-1.90
9	5	L	475.5	160.7	742.9	•	•	•
10	5	R	478.2	181.1	711.8	-.57	11.90	-4.30
11	6	L	524.8	279.0	692.2	•	•	•
12	6	R	471.8	258.7	565.7	-10.60	-7.60	-20.10
13	mean		•	•	•	1.74	13.73	-.35
14	mean (ABS)		•	•	•	8.43	30.50	11.25

$$\text{Diff} = \left[\left[\frac{\text{Right} - \text{Left}}{\frac{\text{Right} + \text{Left}}{2}}\right] \times 100\right] \%$$

mean (ABS) - the mean absolute value

Table 6.4

Comparison of pQCT Results
to Hip and Spine DPX Measurements

		PQCT			DPX			
	Subject	Tot	Trab	Cort	Neck	Ward	Troc	L1-L4
		mg/cc	mg/cc	mg/cc	g/cm2	g/cm2	g/cm2	g/cm2
1	1	245.5	75.3	383.0	.638	.448	.477	.739
2	2	513.2	292.8	580.5	1.029	.993	.902	1.426
3	3	413.2	172.4	624.7	.846	.664	.712	1.008
4	4	286.0	169.6	413.6	.680	.480	.470	.786
5	5	469.3	238.5	596.5	.935	.763	.854	1.079
6	6	332.2	188.3	515.6	.736	.590	.627	.978
7	7	408.1	162.0	635.5	.960	.930	.920	1.126
8	8	351.8	164.6	540.7	.681	.518	.620	.850
9	9	363.9	226.9	427.2	.830	.684	.756	1.254
10	10	271.5	90.1	578.8	.670	.480	.530	.975
11	11	357.5	71.4	682.4	.651	.467	.679	.775
12	12	243.3	92.6	446.4	.650	.435	.515	.824
13	13	312.2	231.6	436.7	.730	.578	.569	1.018
14	14	227.9	107.1	326.6	.750	.590	.580	.960
15	15	186.2	70.7	352.4	.646	.394	.525	.954
16	16	237.9	103.7	436.9	.537	.437	.458	.856
17	17	164.9	104.8	252.2	.640	.440	.440	.860
18	18	408.9	211.9	568.3	.916	.830	.879	1.406
19	19	306.5	112.3	576.0	.722	.533	.644	.955
20	20	400.2	211.5	554.5	.708	.476	.623	.972
21	21	141.4	49.9	292.1	.523	.421	.400	.587
22	22	210.2	109.2	387.7	.700	.361	.583	.908
23	23	303.7	113.3	542.1	.657	.489	.479	.490
24	24	363.3	136.0	622.5	.614	.488	.507	.883
25	25	287.7	101.1	532.1	.708	.518	.628	.797
26	26	364.0	125.6	653.6	.730	.580	.730	.913
27	27	374.6	237.7	478.2	.782	.599	.680	1.386
28	28	185.3	90.7	348.3	.603	.448	.564	.896
29	29	280.4	113.1	453.2	.714	.637	.595	1.018
30	30	323.0	141.9	555.3	.760	.680	.540	1.008
31	31	316.8	95.3	574.9	.744	.588	.618	.870
32	32	247.5	97.5	459.9	.642	.465	.461	.836
33	33	281.4	140.6	428.9	.679	.586	.554	1.020
34	34	180.7	100.2	317.2	.650	.452	.644	.791
35	35	437.0	185.8	685.7	.767	.700	.718	1.139
36	36	335.8	186.2	457.7	.760	.580	.650	1.182
37	37	311.6	208.0	446.8	.736	.595	.615	.907
38	38	393.0	150.5	648.1	.770	.662	.689	1.053
39	39	420.0	191.4	643.5	.898	.789	.690	.871
40	40	378.5	80.7	712.6	.727	.548	.692	.785

continued....

		pQCT			DPX			
	Subject	Tot	Trab	Cort	Neck	Ward	Troc	L1-L4
		mg/cc	mg/cc	mg/cc	g/cm2	g/cm2	g/cm2	g/cm2
41	41	268.7	114.9	475.4	.699	.598	.600	.905
42	42	516.0	279.1	629.4	1.113	.847	.846	1.257
43	43	274.1	183.9	405.5	.656	.548	.610	1.116
44	44	253.1	183.2	354.3	.731	.552	.695	.892
45	45	296.3	139.9	498.8	.587	.365	.480	.800
46	46	551.9	233.6	739.5	.771	.570	.944	1.188
47	47	268.7	184.1	337.2	.710	.430	.560	.884
48	48	195.0	66.0	300.3	.664	.550	.517	.773
49	49	463.1	185.0	713.9	1.018	.979	.913	1.340

Neck - bone mass in the femoral neck
Ward - bone mass in the Ward's triangle
Troc - bone mass in the trochanteric region
L1-L4 - bone mass in vertebrae L1-L4

Figure 6.3

Trabecular pQCT vs. Lumbar Spine DPX

Relatively Good Correlation

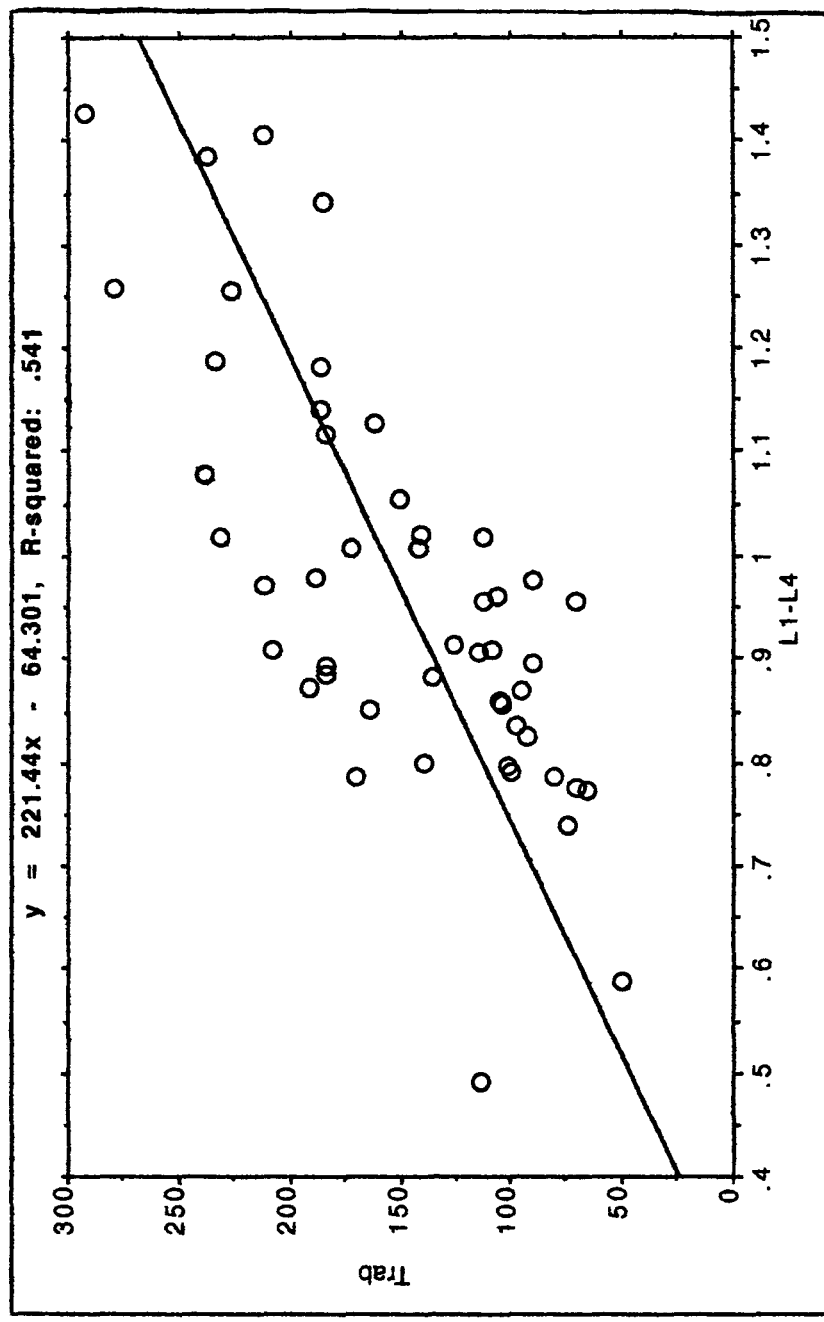

Figure 6.4

Trabecular vs. Cortical Results
(Both Measured using pQCT System)

Poor Correlation

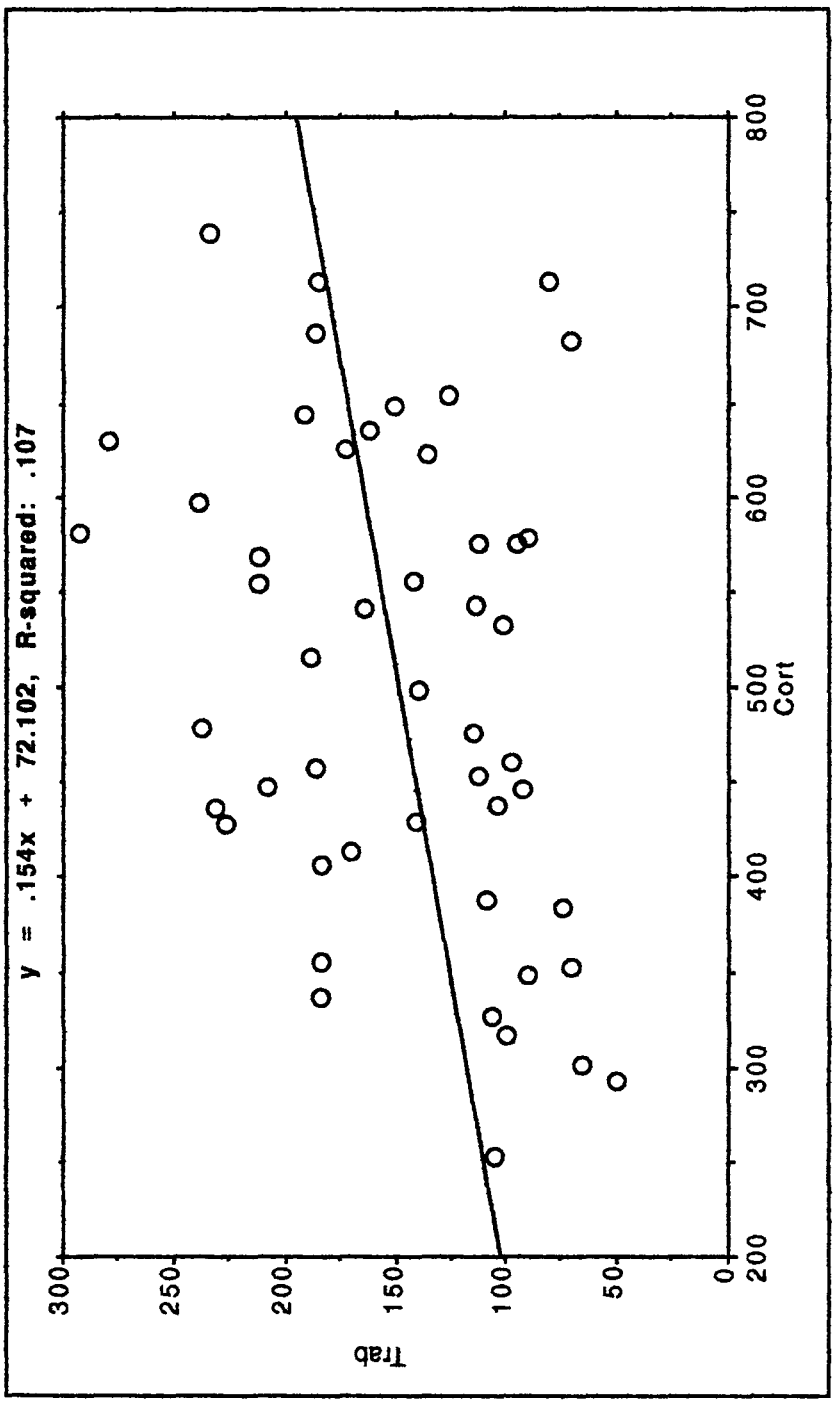

Table 6.5

Correlation Matrix for pQCT-DPX Comparison

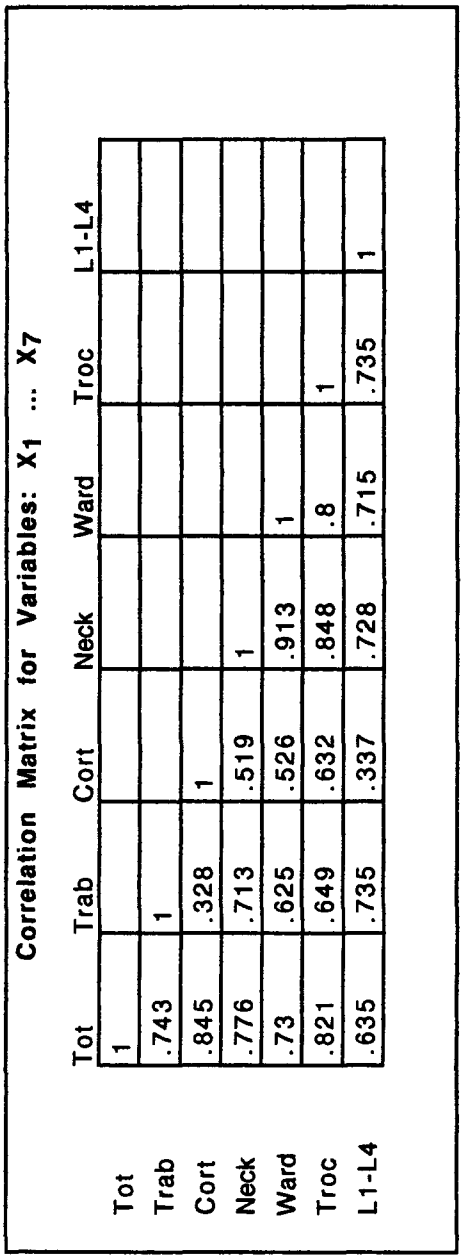

Correlation Matrix for Variables: X_1 ... X_7

	Tot	Trab	Cort	Neck	Ward	Troc	L1-L4
Tot	1						
Trab	.743	1					
Cort	.845	.328	1				
Neck	.776	.713	.519	1			
Ward	.73	.625	.526	.913	1		
Troc	.821	.649	.632	.848	.8	1	
L1-L4	.635	.735	.337	.728	.715	.735	1

the highest correlation with the lumbar spine BMD. As measured by ash weight, trabecular bone makes up 80% of total bone mass in males at the lumbar spine (72% in females) [30]. The radius cortical bone mass shows the best correlation with the bone mass at the trochanter, which is predominantly cortical bone. The percentage cortical bone at the trochanter is 54.3, as measured by Hoiseth et. al. [31]. The worst correlation (0.33) is demonstrated between trabecular and cortical bone at the same site measured by the same technique. Taken together these results indicate that trabecular bone and cortical bone behave differently from each other as bone compartments but each compartment behaves similarly at different anatomical locations. Thus we can postulate that a subject showing a loss of trabecular bone in the distal radius as measured by pQCT would also have a lowered trabecular bone mass in the spine and hip.

There are a number of explanations for the scatter in figures 6.3 and 6.4.

1) There are differences in regional stresses and strains from subject to subject. Those who use their arms frequently for heavy lifting would probably show an elevated bone mass in the radius but perhaps a normal bone mass elsewhere. Those who use their arms little but walk frequently may well display a bone mass in the hip which would probably be quite high compared to the radius.

2) Metabolic bone disorders do not necessarily affect all sites or types of bone equally. The activities of bone cells responsible for remodeling processes in bone are not uniform throughout the skeleton.

3) Local bone mass and fracture risk is dependent on the proportion of trabecular to cortical bone at that site.

4) There is some variation between DPX machines. Some scatter could result from six different machines being used for the 49

subjects. Inter-machine differences are quite small between units from the same manufacturer even with older technology (DPA) [32], and even better for newer DPX models [33].

6.3 A Usable in-vivo Method?

Assuming that an architectural measurement is important in assessing bone strength, pQCT would seem to provide a potential means of quantifying this variable. It measures both bone density, already known to be an important factor, as well as imaging trabecular architecture. But is the resolution sufficient to image the architecture clearly enough for our analytical needs? The manufacturer states the maximum resolution of the machine as .59 mm. This is not enough for our purposes. Trabeculae are on the order of .1 mm thick, with spacings of .2 to .5 mm as can be seen in figure 2.3. Figure 6.5 is an image of a femoral head taken in air to maximize contrast between bone and non-bone material. It confirms the need for higher resolution.

Attempts were made to confirm the stated resolution of the system. Stainless steel meshes with different wire and spacing sizes were scanned, in an attempt to find the smallest size that could be resolved. Unfortunately, these tests were unsuccessful. The software expects a two-component system (soft tissue and bone) and scanning the screens produced errors in calculation. The fact that the thickness of the screen is less than that of the slice is thought to be a problem as well. Aluminum, with a stopping power approximately 9 times less than that of stainless steel, is likely a better material to use as a phantom. A possible viable phantom would be a resin cylinder with holes drilled at regular spacings to allow for the insertion of aluminum rods. Scanning a number of

Figure 6.5

pQCT Measurement of a Femoral Head Taken in Air

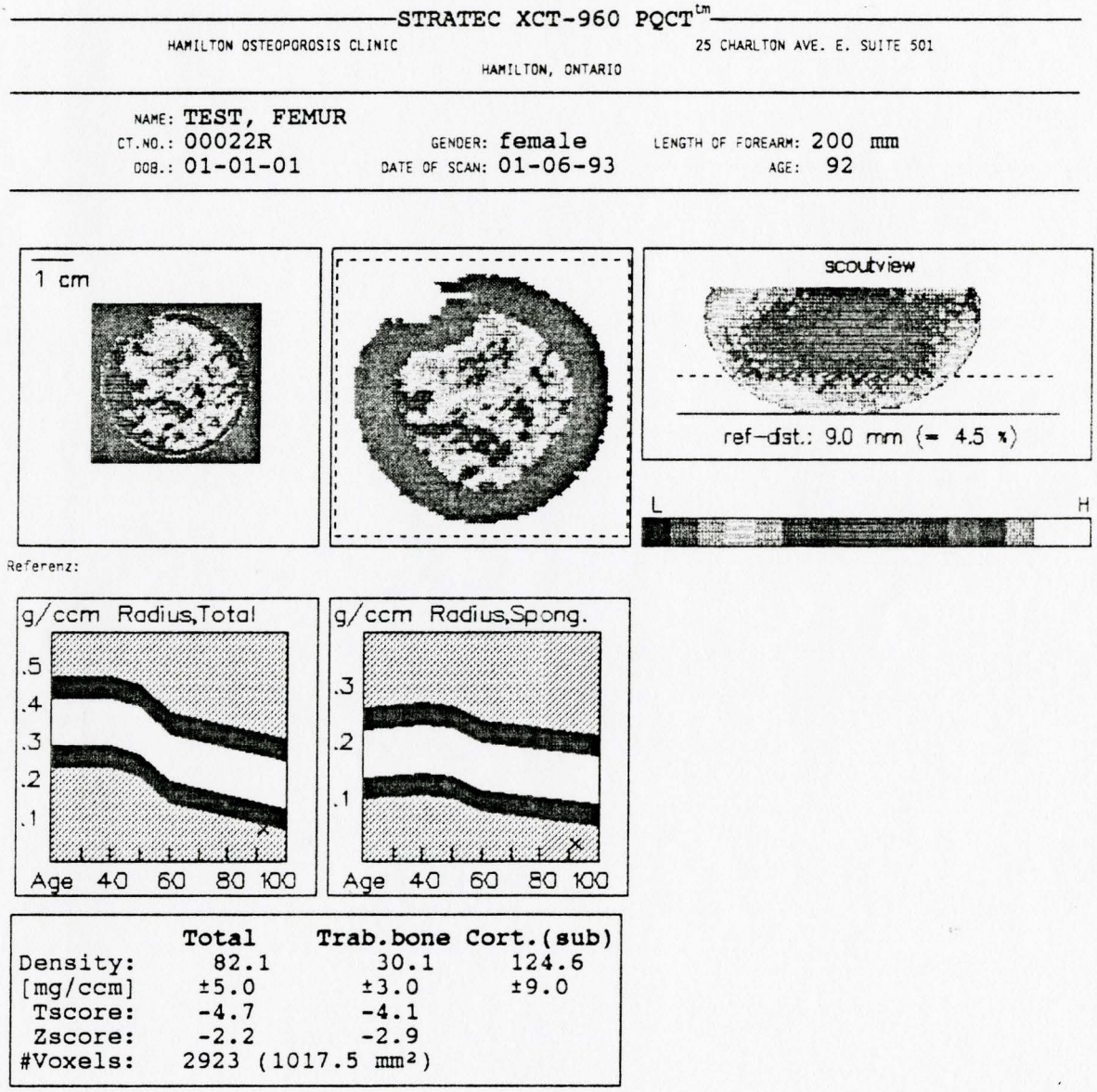

these phantoms with different rod sizes and hole spacings, one could see the minimum rod size and hole spacing at which the system could still resolve the image.

One of the factors contributing to the insufficient resolution is the standard dilemma of balancing image quality and patient dose. Since the machine is not set up to do any in-vitro work, the femoral head was scanned using the same parameters as would be used for a patient. For the purposes of our study, it would have been invaluable to be able to decrease scan speeds, and thus improve the resolution. However, the fact remains that the necessary resolution cannot yet be obtained in-vivo with the current setup.

References

1. T.L. Holbrook, K. Glazier, J.L. Kelsey, R.N. Stauffer, "The Frequency of Occurence, Impact, and Cost of Musculoskeletal Conditions in the United States", Chicago: American Academy of Orthopaedic Surgeons, 1984.

2. S.R. Cummings, J.L. Kelsey, M.C. Nevitt, K.J. O'Dowd, "Epidemiology of Osteoporosis and Osteoporotic Fractures", Epidemiological Reviews, 7,1985: 178-208.

3. J.A. Kanis, D. Aaron, D. Evans, M. Thavarajah, M. Beneton, "Bone Loss and Age-Related Fractures", Experimental Gerontology, 25, 1990: 289-296.

4. M.E. Tinetti, M. Speechley, "Prevention of Falls Among the Elderly",New England Journal of Medicine, 320, 1989: 1055-1059.

5. M.E. Tinetti, M. Speechley, S.F. Ginter, "Risk Factors for Falls Among Elderly Persons Living in the Community", New England Journal of Medicine, 319, 1988: 1701-1707.

6. S.R. Cummings, M.C. Nevitt, "A Hypothesis: The Causes of Hip Fractures", Journal of Gerontology, 44, 1989: 107-111.

7. ----, "Is Osteoporosis Due to Thinning and Porosity of Compact Bone?", Lunar Corporation Publication, March, 1992: 8.

8. M.A. Greenfield, "Current Status of Physical Measurements of the Skeleton", Medical Physics, 19, 1992: 1349-1357.

9. W.S. Browner, D.G. Seeley, T.M. Vogt, S.R. Cummings, "Non-Trauma Mortality in Elderly Women with Low Bone Mineral Density", The Lancet, 338, 1991: 355-358.

10. A.C. Santora, "Role of Nutrition and Exercise in Osteoporosis", The American Journal of Medicine, 82, 1987: 73-81.

11. P.D. Ross, J.W. Davis, J.M. Vogel, R.D. Wasnich, "A Critical Review of Bone Mass and the Risk of Fractures in Osteoporosis",

Calcified Tissue International, 46, 1990: 149-161.

12. B.L. Riggs, H.W. Wahner, E. Seeman, K.P. Offord, W.L. Dunn, R.B. Mazess, K.A. Johnson, L.J. Melton, "Changes in Bone Mineral Density of the Proximal Femur and Spine with Aging: Differences Between the Postmenopausal and Senile Osteoporosis Syndromes", Journal of Clinical Investigation, 70, 1982: 716-723.

13. Li. Mosekilde, Le. Mosekilde, "Iliac Crest Trabecular Bone Volume as Predictor for Vertebral Compressive Strength, Ash Density and Trabecular Bone Volume in Normal Individuals", Bone, 9, 1988: 195-199.

14. Li. Mosekilde, Le. Mosekilde, C.C. Danielsen, "Biomechanical Competence of Vertebral Trabecular Bone in Relation to Ash Density and Age in Normal Individuals", Bone, 8, 1987: 79-85.

15. J.H. Mielke, G.J. Armelagos, D.P. Van Gerven, "Trabecular Involution in Femoral Heads of a Prehistoric (X-Group) Population from Sudanese Nubia", The American Journal of Physical Anthropology, 36, 1972: 39-44.

16. D.H. Kranendonk, J.M. Jurist, H.G. Lee, "Femoral Trabecular Patterns and Bone Mineral Content", The Journal of Bone and Joint Surgery, 54, 1972: 1472-1478.

17. K.S. Jensen, Li. Mosekilde, Le. Mosekilde, "A Model of Vertebral Bone Architecture and its Mechanical Properties", Bone, 11, 1990: 417-423.

18. M. Singh, "Femoral Trabecular Pattern Index for Grading Osteoporosis", 1970, Proceedings of the First Workshop on Bone Morphometry, 1973.

19. W. Remagen, Osteoporosis. Switzerland: Sandoz Ltd.,1989.

20. A.M. Parfitt, "Trabecular Bone Architecture in the Pathenogenesis and Prevention of Fracture", The American Journal of Medicine,

82, 1987: 68-72.

21. J.M. Vaughn, The Physiology of Bone, Toronto, The Oxford University Press, 1970.

22. Weiner, S., Traub, W., "Bone Structure: from angstroms to microns", FASEB, 6, 1992: 879-885.

23. Eanes, E.D., Posner, A.S., "Structure and Chemistry of Bone Mineral", Biological Calcification, 1970.

24. H.M. Frost, ed., The Orthopedic Clinics of North America: Symposium on the Osteoporoses, Toronto, The W.B. Saunders Company, 1981.

25. D.R. Carter, W.C. Hayes, "Bone Compressive Strength: The Influence of Density and Strain Rate", Science, 194, 1976: 1174-1176.

26. R.B. Martin, "Determinants of the Mechanical Properties of Bone", Journal of Biomechanics, 24, 1991: 79-88.

27. D.H. Birkenhager-Frenkel, P. Courpron, E.A. Hupscher, E. Clermonts, M.F. Coutinho, P.I.M. Schmitz, P.J. Meunier, "Age-Related Changes in Cancellous Bone Structure: A Two-Dimensional Study in the Transiliac and Iliac Crest Biopsy Sites", Bone and Mineral, 4, 1988: 197-216.

28. W.G.M. Geraets, P.F. Van der Stelt, C.J. Netelenbos, P.J.M. Elders, "A New Method for Automatic Recognition of the Radiographic Trabecular Pattern", Journal of Bone and Mineral Research, 5, 1990: 227-232.

29. R.W.E. Mellish, M.W. Ferguson-Pell, G.V.B. Cochran, R. Lindsay, D.W. Dempster, "A New Manual Method for Assessing Two-Dimensional Cancellous Bone Structure: Comparison Between Iliac Crest and Lumbar Vertebra", Journal of Bone and Mineral Research, 6, 1991: 689-696.

30. R. Eastell, L. Mosekilde, S.F. Hodgson, B.L. Riggs, "Proportion of

Human Vertebral Body Bone that is Cancellous", Journal of Bone and Mineral Research, 5, 1990: 1237-1241.

31. A. Hoiseth, A. Alho, T. Husby, "Femoral Cortical/Cancellous Bone Related to Age", Acta Radiology, 31, 1990: 626-627.

32. C.E. Webber, "Some Factors which Influence the Evaluation of a Dual Photon Measurement of Lumbar Spine Bone Mineral Mass", Journal of the Canadian Association of Radiologists, 40, 1989: 87-91.

33. N.A. Pocock, P.N. Sambrook, T. Nguyen, P. Kelly, J. Freund, J.A. Eisman, "Assessment of Spinal and Femoral Bone Density by Dual X-Ray Absorptiometry: Comparison of Lunar and Hologic Instruments", Journal of Bone and Mineral Research, 7, 1992: 1081-1084.